Characterization of Aptamers Binding to SARS-CoV-2 Nucleocapsid (N) Protein: A Comparison of Capillary Electrophoresis and Bio-Layer Interferometry

Gurcharan Uppal

A thesis submitted in partial fulfillment of the

requirements for the degree of

Master of Science
in
Chemistry

Department of Chemistry and Biomolecular Sciences

University of Ottawa

Abstract

COVID-19 is caused by the severe acute respiratory syndrome coronavirus 2 (SARS-CoV-2). COVID 19 is detected by RT-PCR tests and serological tests. RT-PCR tests detect viral RNA and require trained individuals to run the test as well as a lengthy analysis time. Serological tests detect antibodies produced in response to viral infection. Rapid antigen detection (RAD) tests, such as the at-home COVID test kits, are quick and easy to run. RAD tests detect viral antigen in the test sample binding to the antibody-coated testing device. However, production of antibodies is a long and costly process. Aptamers can replace antibodies with advantages including low-cost, stability, tunable selectivity, and ability to be chemically modified. Aptamers are short single-stranded oligonucleotides selected for specific targets using Systematic Evolution of Ligands by Exponential Enrichment (SELEX).

This project aims to characterize the binding of aptamers to SARS-CoV-2 nucleocapsid (N) protein using capillary electrophoresis (CE) and compare with bio-layer interferometry (BLI). DNA aptamers were selected via SELEX and screened using BLI in which protein was immobilized on the BLI sensor tip and dipped into aptamer solution. Three aptamers specific to N protein were selected for further binding affinity (Kd) determination.

In CE, the aptamer and protein are free in solution to bind and unbind, providing an alternative approach in characterizing the binding. A greater K_d was observed with CE compared to BLI. Using CE, the apparent Kd of the 3 aptamers was determined to be 18 ± 4 nM, 45 ± 11 nM, and 32 ± 7 nM, respectively. When tested with BLI, the apparent K_d were 4.83 ± 0.63, 4.51 ± 0.87, and 2.91 ± 0.59 nM, respectively. This discrepancy in affinity can be due to steric differences between immobilized (BLI) and in solution (CE) binding, buffer composition and stability of aptamer structures, or buffer pH and difference in electrostatic interactions. All three of these variables will impact binding and the calculated K_d. This work offers insight into aptamer affinity when used in a different system from which they were selected. This work would lead to a better understanding when employing aptamers to different assays and assay mediums.

Acknowledgements

I would like to express my utmost gratitude and appreciation to Dr. Maxim Berezovski for all his support during my graduate studies. Dr. Maxim Berezovski has helped me improve and hone my research and professional skills, including my critical thinking, writing, and laboratory skills. His motivation, work ethic, and determination has inspired me to work hard and strive for my goals throughout my studies and moving into the future.

I would also like to express my gratitude to Dr. Zoran Minic for all his feedback and advice over these past couple of years.

I am grateful for my friends and lab mates for their continuous feedback, encouragement, and friendship. I would like to express my thanks to Rochelle D'Mello for her kind heart and continuous support throughout my time at uOttawa. Thank you to Yuxuan (Carlos) Gu for sharing both his joy for basketball and for his CE comraderie.

Finally, I would like to thank my parents and my family. My parents have always been available to support and motivate me to try my best and have given me the strength to be resilient. And thank you to my brother for encouraging me and being a great role model. In particular, I would like to thank them for their unconditional love, unwavering support, and countless sacrifices.

Statement of Contributions

Experimental Design

The project design and idea were conceived by Dr. Maxim Berezovksi. Suttinee Poolsup selected aptamers to SARS-CoV-2 N protein providing the aptamer clones for the basis of this work. I optimized the capillary electrophoresis experiments through literature research and my experimental results. I worked with Suttinee Poolsup to design the bio-layer interferometry BLItz protocol for the comparison with the developed capillary electrophoresis method.

Experiments

Capillary electrophoresis method optimization was completed by me. The determination of K_d, $K_{on,}$ and K_{off} from CE was completed by me. Preliminary BLI results with ammonium acetate buffer was completed by me and Suttinee Poolsup. The determination of K_d, K_{on}, and K_{off} using BLI was completed by Suttinee Poolsup. SARS-CoV-2 nucleocapsid protein was expressed and purified by Emil Zaripov and Yuxuan (Carlos) Gu.

Written Report

This thesis was written by me, edited by Dr. Zoran Minic and Dr. Maxim Berezovski, and reviewed by Dr. Maxim Berezovski.

List of Figures

List of Tables

Table of Contents

1. Introduction

1.1. SARS-CoV-2 and Nucleocapsid (N) Protein

Severe acute respiratory coronavirus 2 (SARS-CoV-2) is the causative agent of the COVID-19 pandemic. While for many people COVID-19 does not carry the same adverse outcome as it did early in the pandemic, the reality is that COVID-19 continues, and will continue, to play a major role for the foreseeable future. COVID-19 currently has higher annual morbidity than a severe influenza season (US); moreover, many people suffer from long- and short-term COVID-19 illness and associated complications.[1] With the ever-present possibility of a new variant, there is a continuing and evolving need for strategies for monitoring and combating COVID-19.

SARS-CoV-2 consists of four structural proteins and the viral RNA genome (Figure 1). The four proteins include envelope (E), membrane (M), nucleocapsid (N), and spike (S) protein. N protein binds to the RNA genome which is enclosed in a lipid membrane containing E, M, and S proteins. Infection occurs through the binding of S protein to the angiotensin-converting enzyme 2 (ACE2) receptors on the host cell.[2] The S protein, specifically subunit S1, contains the receptor binding domain. Based on this knowledge, and from previous studies of SARS-CoV-1 and related MERS-CoV, S protein was identified as an ideal target for theragnostic development early on in the pandemic.[3–5] Further along into the pandemic, reports showed multiple mutations in the S protein and receptor binding domain.[6,7] While a suitable initial target, the emergence of variants can limit the effectiveness of previously developed strategies targeting S protein.

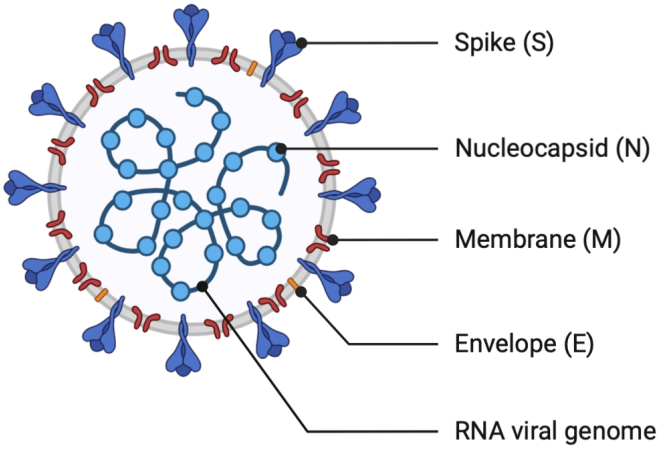

Figure 1. SARS-CoV-2 virus structure highlighting the viral genome and 4 major structural proteins: spike (S), nucleocapsid (N), membrane (M), and envelope (E).

N protein is another suitable target and this protein displays a high copy number (~1000 per viral particle) and is highly expressed early on in infection.[4,6] The N protein is responsible for the packing of SARS-CoV-2 genomic RNA. This multi-domain RNA-binding protein shares substantial sequence conservation with other coronavirus nucleocapsid proteins. Across a range of coronavirus models, N protein has shown to undergo self-association, interaction with other proteins, and interaction with RNA in a highly multivalent manner. The N protein is divided into five domains: N terminal domain (NTD), RNA binding domain (RBD), central linker, dimerization domain, and C-terminal domain (CTD).[8] All five domains are predicted to bind RNA.[8–12] Both the NTD and linker domains have been shown to drive RNA binding through possible nonspecific binding which may also contribute to RNA specificity.[8] The proposed model for genome packaging facilitated by N protein is instigated by a single-genome condensate formed via N protein-gRNA interaction driven by a small number of high-affinity sites. The condensate undergoes subsequent maturation leading to virion assembly.[8] Additionally, the presence of multiple RNA-binding domains is not only relevant to the genome packaging but can also have consequences for interactions with other viral and host biomolecules.[9] Coupled with the substantial sequence conservation, N protein is a relevant and suitable target for SARS-CoV-2 studies.[13]

1.2. Applications of Aptamers with COVID-19

Since the pandemic's onset, gold standard methods for COVID-19 detection have been established. Reverse transcriptase polymerase chain reaction (RT-PCR) is the primary diagnostic tool for active infection.[6] RT-PCR tests detect viral RNA collected via nasopharyngeal swabs. Nucleic acid tests provide superior sensitivity and specificity for viral detection compared to serological tests. As such, RT-PCR is highly accurate in recognizing SARS-CoV-2 over common respiratory pathogens. However, overall RT-PCR workflow and turnaround time can exceed two days and runs the risk of reduced specificity through cross-contamination.[14] Additionally, these tests require trained individuals in a laboratory setting. While RT-PCR excels in sensitivity and specificity, it falls short in terms of time and training costs.

Parallel to nucleic-acid detection are serological tests. These immune-based assays measure the antibodies generated by the body's immune response against virus infection.[15] Rapid antigen detection (RAD) tests, such as the at-home test kits, are a quick and simple type of serological test. RAD tests detect viral antigens in the test sample that bind to the antibody-coated testing device.[16] These tests are highly accessible, and allow for self-monitoring and tracking of viral infection. Serological tests have limited use during early infection because the immune response is still building and may be below detectable concentrations. Where serological tests excel are ease of use, quick results, minimal costs, and availability in clinical and non-clinical settings.[15] One possible drawback is that antibodies are not ideal for large-scale production. Antibodies are produced by inducing an immune response in a lab animal and then collecting the antibodies from the animal's serum after a few weeks. This is an expensive and lengthy process.

Aptamers provide an excellent alternative to antibodies, with several advantages including low-cost production, precise chemical modification, easy storage, and reversible heat-denaturation.[17] Aptamers are short single-stranded RNA or DNA molecules which bind to their targets with similar or higher affinities as antibodies. They interact with their target similarly to antibodies via hydrophobic, electrostatic, hydrogen bonding, and van der Waals interactions.[18] Aptamers are designed by an artificial method called Systematic Evolution of Ligands by Exponential Enrichment (SELEX). Several methods of SELEX have been suggested for aptamer optimization;

the general scheme is shown in Figure 2. In shirt, an oligonucleotide library is incubated with the target molecule of interest. The oligonucleotides with high affinity to the target bind to the molecule, while those with low affinity are removed from the pool. The high-affinity sequences are recovered, and this process is repeated until an aptamer with high specificity to the target is generated. Aptamers have great potential for targeted diagnosis, therapeutics, and drug delivery.[4,18]

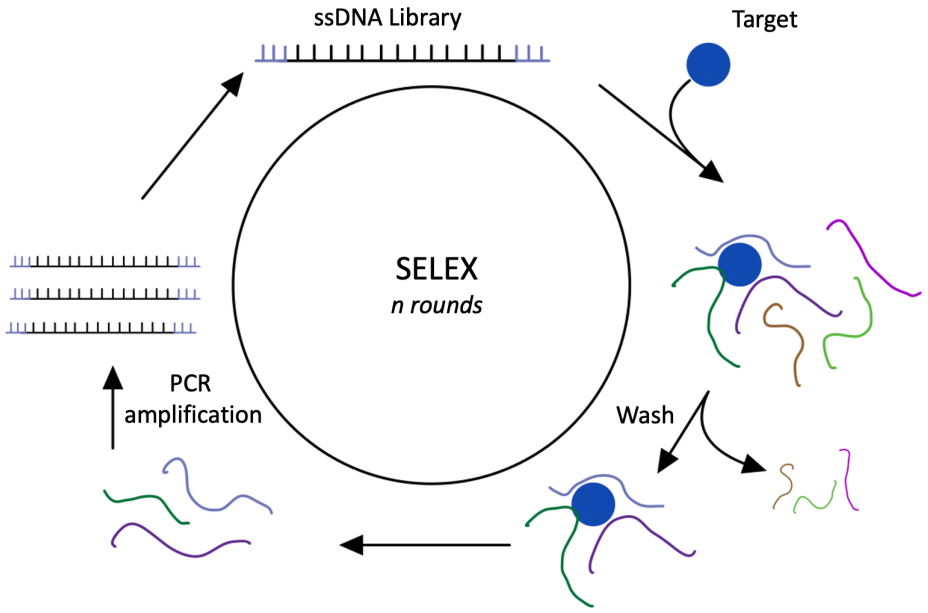

Figure 2. General scheme of Systematic Evolution of Ligands by Exponential Enrichment (SELEX). An initial oligonucleotide library is incubated with the target. There is partitioning of sequences which bind and do not bind to the target. Those sequences which bind are amplified and used in the next round of selection.[19]

1.3. Capillary Electrophoresis

Capillary electrophoresis (CE) is a widely used analytical method in biology and medicine, with over 10 000 CE articles published in *Analytical Chemistry* alone since 2012.[20,21] Capillary electrophoresis is defined as the differential movement of ions by attraction or repulsion in an electric field.[22] The primary components of basic CE instrumentation include a narrow fused silica capillary, two buffer vials, and a sample-introduction system, a high-voltage power supply, a temperature-control system, and a detector (Figure 3).[22,23] Where CE contrasts from other types of electrophoresis, for example, gel-electrophoresis, CE separation is done in solution within the narrow-glass capillary.

The basic principle of a CE run begins with each side of the high-voltage power supply connected to two electrodes. Each end of the pre-electrolyte-filled capillary, along with the electrodes, is dipped in buffer vials. The electrodes induce an electric field to initiate migration of the sample from the anode to the cathode. There is a small window near the cathode end which allows the sample to be detected using a detector such as laser-induced fluorescence (LIF).[22]

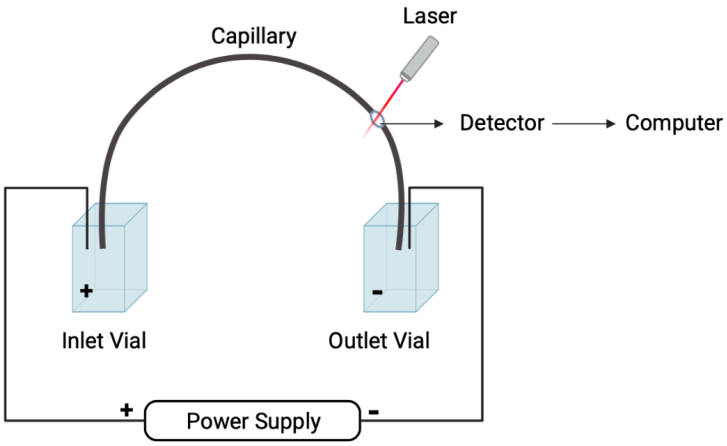

Figure 3. Basic components of CE instrumentation.

A fundamental feature of CE is electroosmotic flow (EOF). EOF is the bulk flow of solution through the capillary. This EOF is achieved by applying a high-voltage to an electrolyte-filled capillary and is the result of the surface charge on the inner capillary wall. The fused silica capillary surface consists of numerous silanol groups (SiOH) that can exist in deprotonated form (SiO^-). Through a series of washes and then filling the capillary with electrolyte (also called running buffer), a negatively charged inner wall (predominantly SiO^-) is achieved. Positive ions build up near the wall surface to maintain charge balance forming a diffuse double-layer. When voltage is applied, the positive ions of the diffuse double-layer are attracted toward the cathode. This movement drags the bulk solution in the capillary toward the cathode. The movement of the bulk solution is called EOF and the magnitude of EOF will overpower any attraction of analytes to the anode, which results in all analytes reaching the detector. The mobility of an analyte through the capillary is the result of its inherent electrophoretic mobility and EOF.[22]

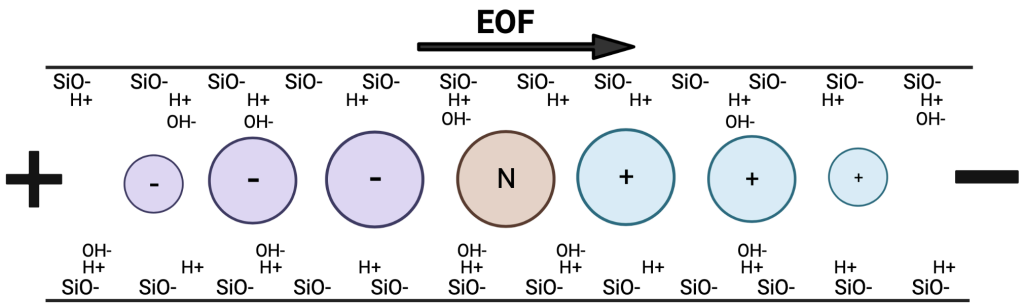

Figure 4. Migration order of analytes through a capillary in an applied field and EOF conditions. Where small, positive analytes migrate relatively faster than neutral analytes, followed by negative analytes.

The charge and radius of a sample affect its mobility through a capillary. Positive ions will move toward the cathode with the flow of EOF, while negative ions will be pulled toward the anode, pushing against the flow of EOF. EOF is stronger than the negative ion-anode attraction and the negative ion will ultimately be pulled toward the detector, though at a slower rate than a positive ion. Larger molecules experience greater interactions and friction, and thus larger hindrance through the capillary. As such, the larger molecules have a decreased velocity toward their respective electrode. This results in a relative migration pattern of small positive ions, large position ions, neutral molecules, large negative ions, and small negative ions, from the shortest to longest migration time (Figure 4).[22]

1.3.1. Kinetic Capillary Electrophoresis

Kinetic capillary electrophoresis (KCE) is the use of capillary electrophoresis with species that interact to determine the affinity of interacting species. This process involves two or more interacting species, which will form a variety of peaks. These peaks, typically one per species, and one per interaction, can be analyzed to determine the association and dissociation rate constants, and measure of affinity (dissociation constant, K_d) of the interacting species.[21] This can be used to study aptamer-protein interactions.

1.3.2. Nonequilibrium Capillary Electrophoresis of Equilibrium Mixtures (NECEEM)

Nonequilibrium capillary electrophoresis of equilibrium mixtures (NECEEM) is a type of KCE. The sample plug for NECEEM contains an equilibrium mixture comprising the ligand, target, and the

ligand-target complex[21]. Each of these components migrates at a different velocity based on relative size and polarity, leading to multiple peaks, one for each electrophoretic component. Generally, the ligand on its own will have the slowest velocity through the capillary, because it is typically a small, negatively charged compound and therefore experiences the most interactions with the anode, and fewer wall interactions. Conversely, the target protein generally experiences a faster velocity due to its size and polarity, and the complex is found between the protein and ligand.[21]

NECEEM is a homogenous separation method that uses differential mobility to separate ligand from ligand-target complex in a free solution. NECEEM does not assume equilibrium in a reaction and acts as a kinetic method, where measurements of association rate (k_{on}) and dissociation rate (k_{off}) can be determined.[21] An ideal electropherogram (Figure 5) will show visible peaks for free ligand (A1), ligand-target complex (A2), and complex dissociation (A3).

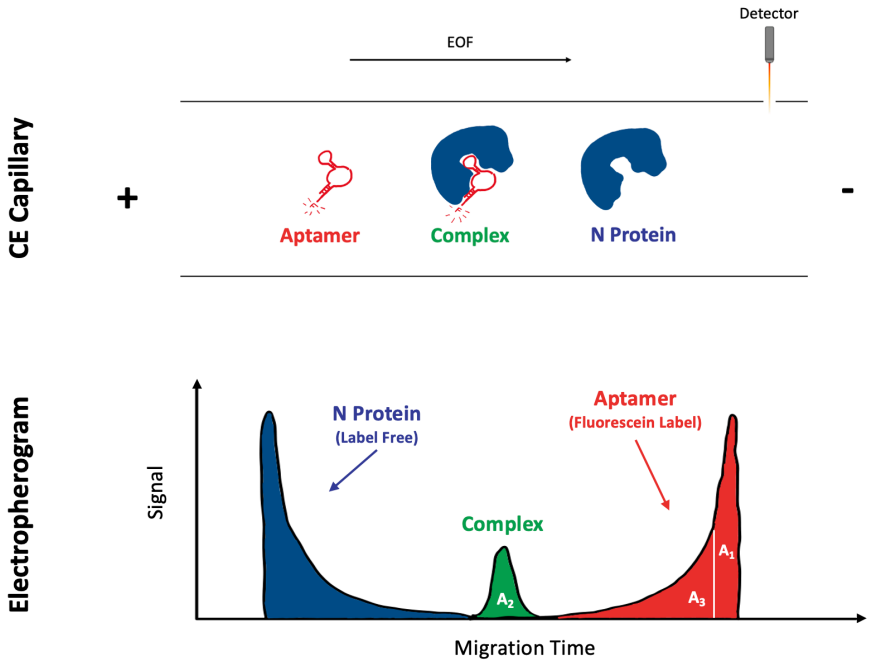

Figure 5. NECEEM curve and respective areas. A homogeneous mixture will present three main species areas. A_1 depicts a free ligand (aptamer), A_2 indicates ligand-target complex formation, and A_3 is the free ligand that has previously been in complex, representing complex dissociation.

1.4. Bio-layer Interferometry

Bio-layer interferometry (BLI) is an optical technique used to measure molecular interactions, such as binding events, in real-time and label-free. BLI measures the interference of light reflected from two surfaces: a layer of biomolecules on the sensor tip and an internal reference layer. Any change to the thickness of the bio-layer causes a shift in the interference pattern, which can be used to determine the kinetics of association and dissociation. BLI is a versatile technique that can be applied to a range of biomolecular interactions such as protein-protein, aptamer-protein, and ligand-protein interactions.[24–26] The technique is relatively simple to use and provides real-time data, making it a valuable tool for deducing molecular interaction information.

The principle of a label-free BLI experiment relies on the immobilization of one biomolecule (e.g., L) on a biocompatible coated sensor surface. The sensor is dipped in a solution containing the binding partner (e.g., T). As the molecules interact, the number of molecules that bind to the sensor tip increase, resulting in a change in bio-layer thickness and associated interference pattern (Figure 6).[24–26] The binding response is displayed in a sensorgram.

A BLI system, such as the FortéBIO BLItz system, consists of a gold-coated biosensor tip that is functionalized with a capture molecule that is specific to the target molecule to be immobilized. The biosensor tip is held in the instrument unit, which houses the optical components and electronics for data acquisition and analysis.[25] The BLItz system allows for a simple dip-and-read protocol.

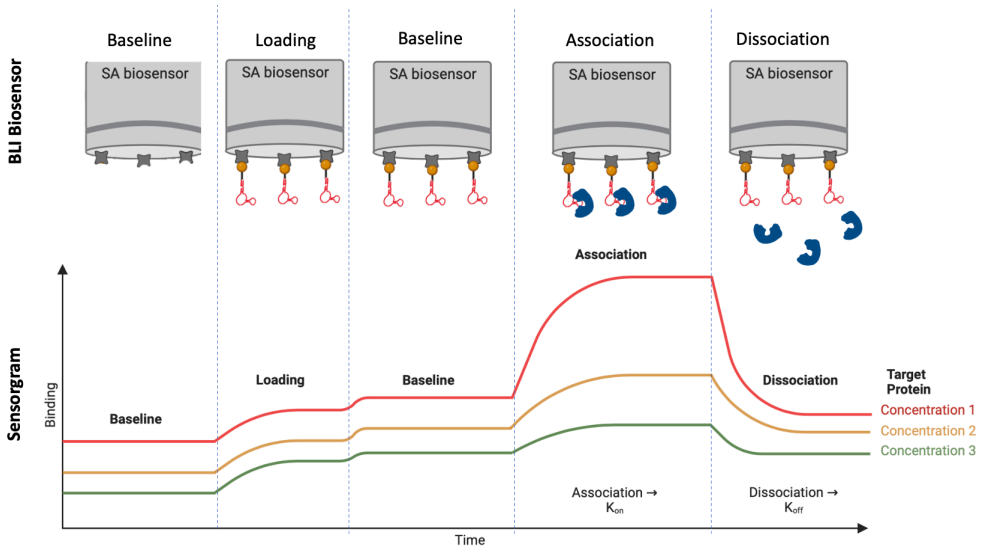

Figure 6. Principle of BLI and the interference pattern change due to biomolecules binding to the immobilized ligand. Baselines are completed in assay buffer, the aptamer is loaded onto the biosensor, the biosensor is dipped into the protein solution and then association occurs followed by dissociation in the assay buffer.

1.5. Heterogenous vs. Homogenous Techniques

The studies of biomolecular interactions are not complete without measurements of affinity. Affinity methods are used heavily in biomedical diagnostics and drug development. The two classes of affinity methods include separation-free and separation-based affinity methods. Separation-free is suitable for affinity measurements while separation-based is suitable for affinity measurements and affinity purification.[21,27] The focus of this thesis is separation-based. Separation-based methods are centered on the physical separation of free ligand (L) or free target (T) from the complex (L•T). Depending on how the separation of L (or T) from L•T is achieved, the method can be further classified as homogenous or heterogenous.

Homogenous methods separate L from L•T in solution. This is achieved through differences in mobility. The difference in mobility can be induced by centrifugal or electrostatic forces. The major limitation of homogenous methods is defining the appropriate conditions to separate L from L•T in solution. Despite this, homogenous methods are preferred for affinity measurements.[21] NECEEM is an example of a homogenous method.

On the other hand, heterogenous methods separate L from L•T on the surface of a solid substrate, such as a filter, chromatographic support, or biosensor. BLI is an example of a heterogeneous technique. The advantage of heterogenous methods is the simplicity of separation, because one species (either L or T) is immobilized on a solid support there is clear separation from L•T. However, the immobilization of L or T to a surface is associated with certain limitations. The immobilization procedure can be expensive and challenging. Once immobilized, molecules often degrade rapidly and immobilization may affect the affinity of L to T. Lastly, the introduction of a surface may induce non-specific binding making the affinity measurements inaccurate.[21,27]

1.6. Rationale and Thesis Objective

This project aims to characterize the binding of aptamers to SARS-CoV-2 nucleocapsid (N) protein using capillary electrophoresis (CE) and compare it with the characterization using bio-layer interferometry (BLI). Aptamers bind with a certain affinity to their biomolecular targets. The affinity can be influenced by conditions such as temperature, ionic strength, cofactors such as Mg^{2+}, pH, etc. Hence, a K_d value alone does not tell the full story. Even more challenging is to compare the K_d values obtained from different techniques, especially if experimental conditions differ.

CE and BLI were chosen as techniques to characterize the aptamers. Although they are two orthogonal methods, the methods encompass two common applications of aptamers. BLI is a heterogenous technique that simulates an aptamer binding to an immobilized binding partner. This is similar to a surface protein on a virus in which the protein is locked in a certain orientation with only a portion of the protein surface available for binding. A surface protein is an ideal aptamer target in situations where the viral body is kept intact. However, if the virus is lysed, then all proteins (surface and internal) are in solution. CE is a homogenous separation-based method in which the binding is occurring in solution. In summary, BLI utilizes a rigid, immobilized constituent, while CE utilizes both binding molecules in solution.

In this project, aptamers were selected via SELEX using immobilized protein to allow for the partitioning of bound and unbound sequences. Binding was screened using BLI where the protein was immobilized on the BLI sensor tip and dipped into a solution containing the aptamer solution. Three aptamers specific to N protein were selected to determine their binding affinity (K_d) using the two techniques described above. This work offers insight into aptamer affinity when used in a different system from which they were selected. This leads to a better understanding when employing aptamers to different assays and assay mediums.

2. CE Method Optimization

SELEX was completed using a PBS buffer with 1 mM Ca^{2+} and 0.5 mM Mg^{2+} at pH7.4. The final round of SELEX was screened using BLI. The three aptamers with the best binding (tNSP1, tNSP2, and tNSP3) were selected and then tested to determine their K_d using BLI and CE. However, BLI conditions may not be ideal for running CE. The goal of this chapter is to determine the optimal CE conditions for determining K_d of the selected aptamers. The parameters to be optimized include running buffer, CE sample vials coating, and the addition of Ca^{2+} and Mg^{2+} to the sample buffer.

2.1. Optimal Run Buffer

2.1.1. Introduction

To determine the optimal run buffer, phosphate, ammonium acetate, and ammonium bicarbonate buffers were tested. The selection of aptamers was done in the PBS buffer. However, the high concentration of salts in the PBS is not suitable for CE.[22] In this case, phosphate buffer was chosen as a CE alternative. The pH range was selected as pH 7.2-7.4 to mimic the aptamer selection conditions. Additionally, two ammonium-based buffers were also tested. The ammonium buffers are volatile and MS-compatible. The criterion of CE-MS compatibility was chosen to allow for future work using MS detection. With a pKa of 6.4 (HCO_3^-), ammonium bicarbonate is a CE-MS buffer that falls within the pH 7.2-7.4 range.[28] Lastly, the commonly used CE-MS buffer is ammonium acetate.[28,29]

2.1.2. Methods

Capillary Electrophoresis (CE) Method (NECEEM)

NECEEM was performed with a CE instrument (P/ACE MDQ, Beckman-Coulter) with laser-induced fluorescence (LIF) detection (488 nm excitation, 520 nm emission). An uncoated fused-silica capillary was used with the following dimensions: 60 cm × 75 µm i.d. × 350 µm o.d. The length from the injection end to the detection window was 50 cm. Electrophoresis was run with a positive electrode at the injection end and an electric field of 416 V/cm. The run buffer was 10 mM ammonium bicarbonate pH 7.36, 10 mM phosphate buffer pH 7.22, or 10 mM ammonium acetate pH 9.20. The capillary was rinsed with a succession of 1.0 mM SDS, 100 mM HCl, 100 mM NaOH, and MS water. The samples were injected with a 0.5 psi pressure for 15 s into the capillary which was prefilled with the run buffer.

Ohm Plot

To determine the applied voltage used in capillary electrophoresis with a 10 mM ammonium acetate pH 9.00 buffer, an Ohm plot was constructed. Using P/ACE MDQ, Beckman-Coulter CE-LIF, 60 cm × 75 µm i.d. × 350 µm glass-silica capillary, and 32Karat software the following procedure was performed. The capillary was rinsed with 0.1 M HCl, water, 0.1 M NaOH, water, and the running buffer, each for 1 minute at 20 psi. The separation was performed on a range of 1-30 kV in the running buffer, with the separation voltage increasing by 1 kV increments every 0.3 minutes.

2.1.3. Discussion and Results

10 mM Phosphate pH 7.22 buffer

As a test sample, tNSP2 aptamer was used. The aptamer migrated at 23 min with a peak height of 1.9 RFU (Figure 7). This migration time is useful in determining the binding of the aptamer to N protein, because the longer migration time allows for better resolution of the aptamer and

aptamer-protein complex peaks. However, a long migration time results in a long run time. When working with biomolecules, there is the possibility of degradation as the sample stays at room temperature for prolonged periods of time. Additionally, if each run is long, then the overall experiment is not time efficient.

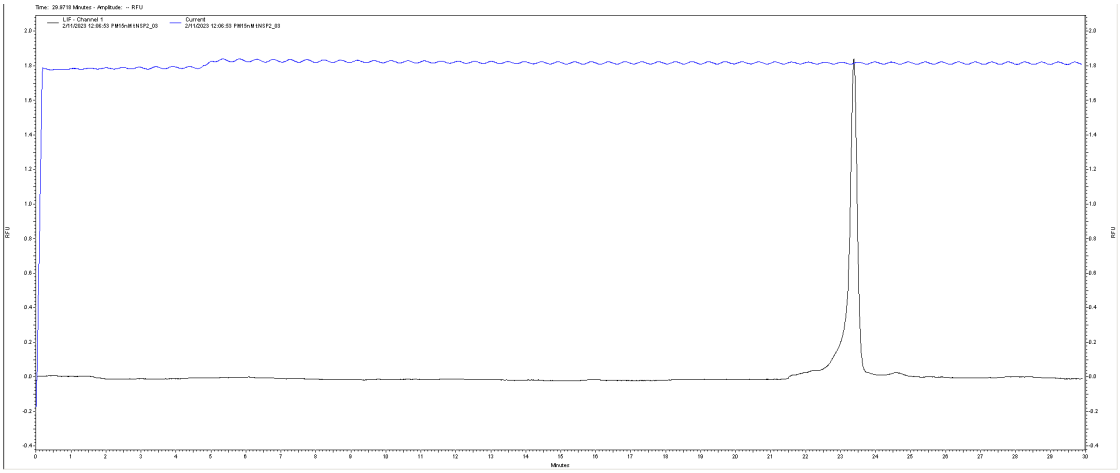

Figure 7. Electropherogram of 15nM tNSP2 aptamer. Separation of 25KV in 10mM phosphate buffer. Current shown in blue (μA), LIF signal shown in black (RFU).

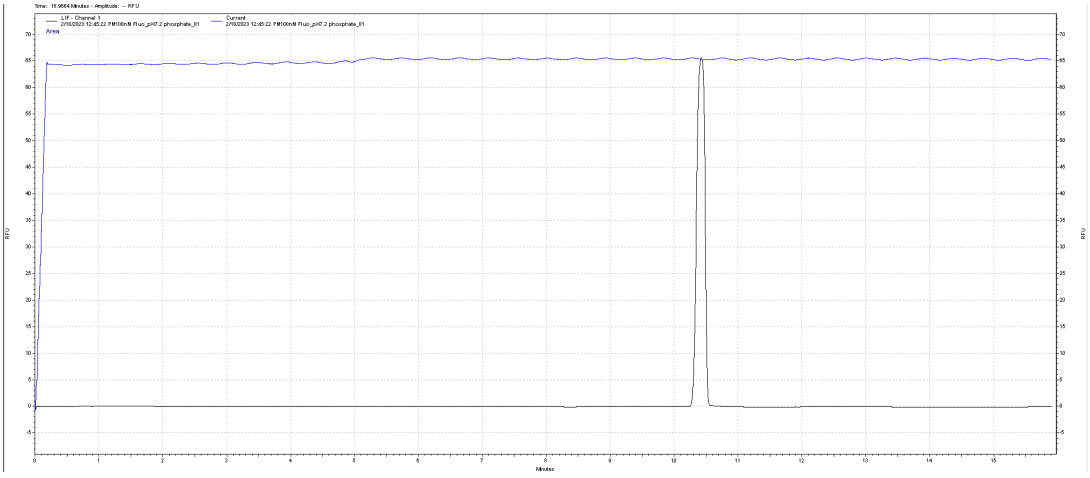

Figure 8. Electropherogram of 100nM fluorescein. Separation of 25KV in 10mM phosphate buffer. Current shown in blue (μA), LIF signal shown in black (RFU).

Neutral molecules migrate with EOF. Therefore, fluorescein was used to estimate EOF as a close-to-neutral molecule with a peak excitation at 495 nm and peak emission at 520 nm. Fluorescein migrates at 10.4 min (Figure 8). The affective mobility (μ_a), in this case approximately μ_{EOF}, was calculated to be 4.8cm/min (length to detector/migration time).

10mM Ammonium Bicarbonate pH 7.36 buffer

The migration time of the tNSP2 aptamer was significantly faster at 10.9 min and an observed peak height of 5.4 RFU (Figure 9). The EOF was estimated using 100nM fluorescein (Figure 10), which had a migration time 6.7 min. The calculated EOF was 7.5 cm/min. This is approximately 1.5x the speed compared to the phosphate buffer. With the aptamer migration time close to 11 min (Figure 9), there is still sufficient time to allow for fully resolved aptamer and aptamer-protein complex peaks. Additionally, an 11 min migration is much more time-efficient compared to the phosphate buffer.

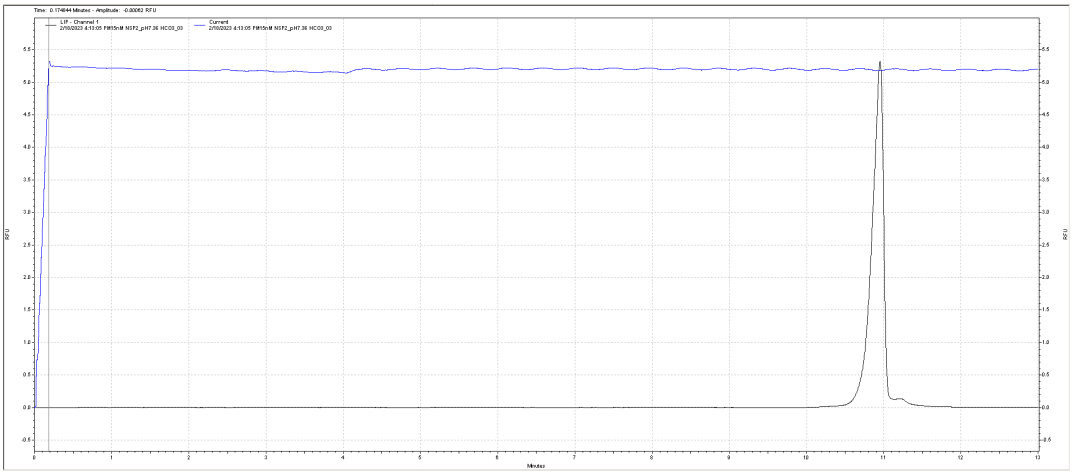

Figure 9. Electropherogram of 15nM tNSP2 aptamer. Separation of 25KV in 10mM ammonium bicarbonate buffer. Current shown in blue (μA), LIF signal shown in black (RFU).

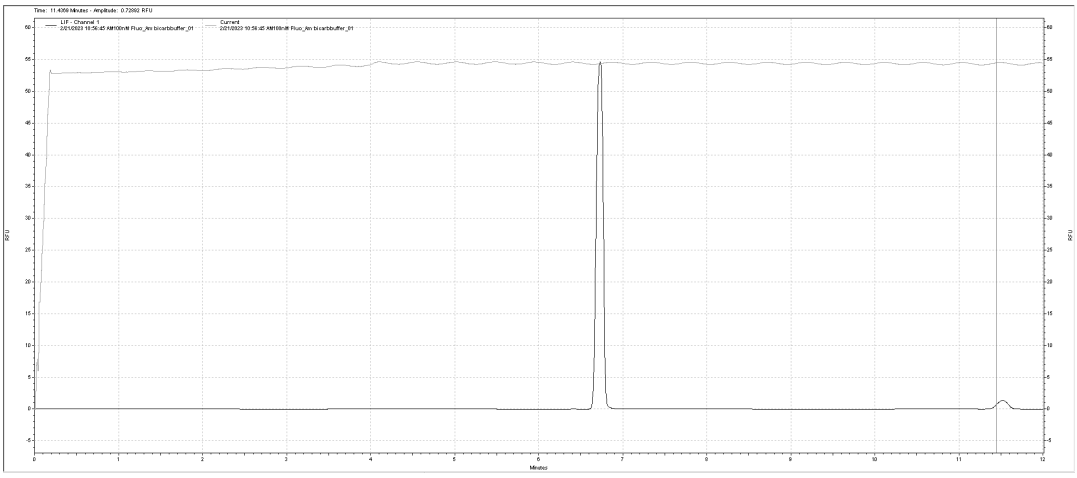

Figure 10. Electropherogram of 100nM fluorescein. Separation of 25KV in 10mM ammonium bicarbonate buffer. Current shown in blue (μA), LIF signal shown in black (RFU).

The migration time in the ammonium bicarbonate running buffer was deemed acceptable in terms of being time efficient, while still allowing time for resolution. Next, the reproducibility of the migration time was tested. When testing K_d for each aptamer, six concentrations of N protein are to be tested in triplicate. This would correspond to an entire day of running CE per aptamer, so it is imperative that the results can be compared from the morning all the way to the last run. As seen in Figure 11, the migration time for the tNSP2 aptamer peak shifted significantly throughout the replicates. This ranged from 6.3 min to 13.5 min with the later migrating peaks appearing shorter and wider. Shifting migration time might be the result of the stability of the ammonium bicarbonate buffer.

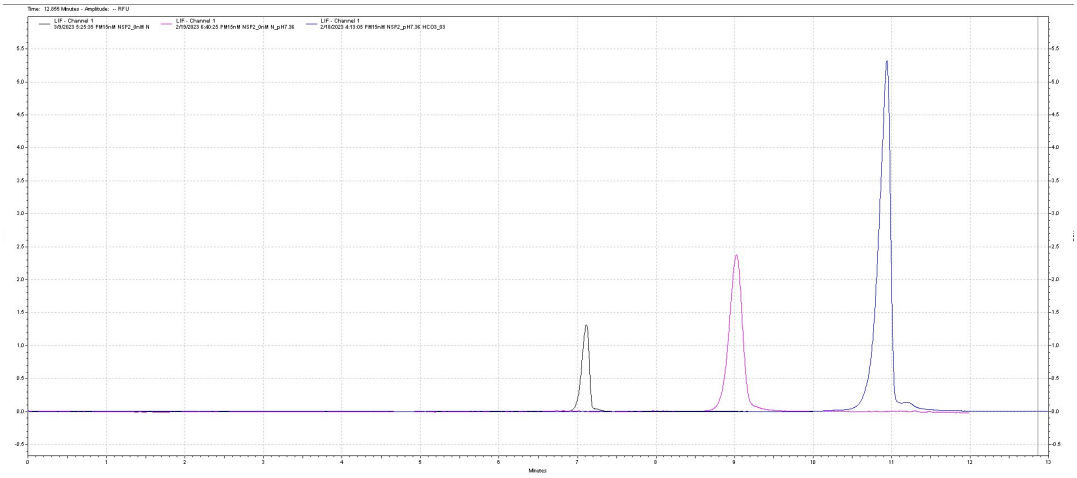

Figure 11. Stacked electropherogram of 15nM tNSP2 aptamer. Separation of 25KV in 10mM ammonium bicarbonate buffer, with replicate one in blue, replicate two in purple and replicate three in black.

Ammonium bicarbonate buffers with gaseous ammonia, carbon dioxide, and water. As the buffer sits in the CE, the vial cap is not an airtight seal. It is possible that the buffer equilibria are affected. This might be through contact with the air while it sits in the CE as well as when the capillary is prefilled with the buffer using pressure injection. This hypothesis was tested by checking the pH of the buffer after running. Over the timespan of one week, the pH of the stock buffer solution had changed to pH 7.86, compared to pH 7.36 when the buffer was newly prepared.

10mM Ammonium Acetate pH 9.00 buffer

The migration time of the tNSP2 aptamer was faster still at 7.10 min and a peak height of 1.31 RFU (Figure 12). The EOF was estimated using 100nM fluorescein (Figure 13), which had a migration time of 5.4 min. The calculated EOF was 9.3 cm/min. With the aptamer migration time being close to 7 min (Figure 12), it is the fastest migration of the buffers tested. There is still sufficient time to allow for fully resolved aptamer and aptamer-protein complex peaks as hypothesised and later evidenced in the K_d experiments (see Chapter 3).

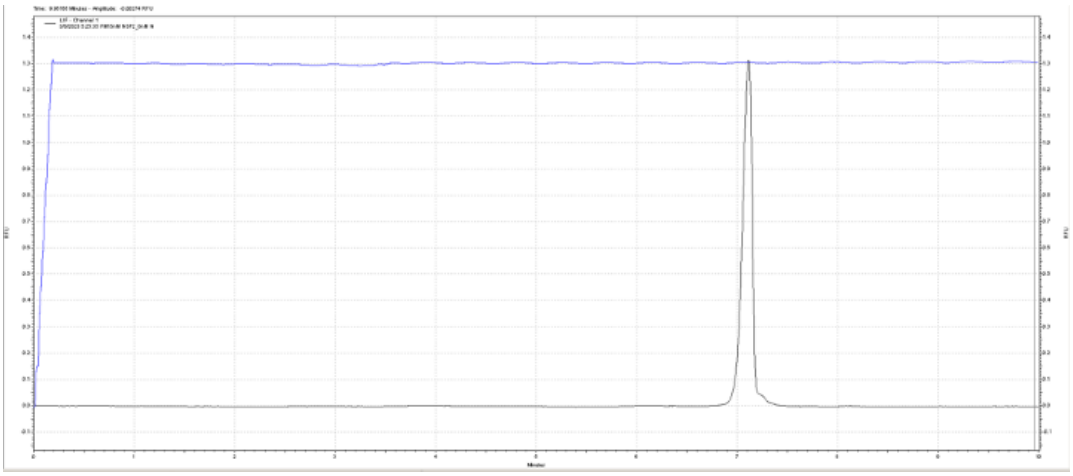

Figure 12. Electropherogram of 15nM tNSP2 aptamer. Separation of 25KV in 10mM ammonium acetate buffer. Current shown in blue (μA), LIF signal shown in black (RFU).

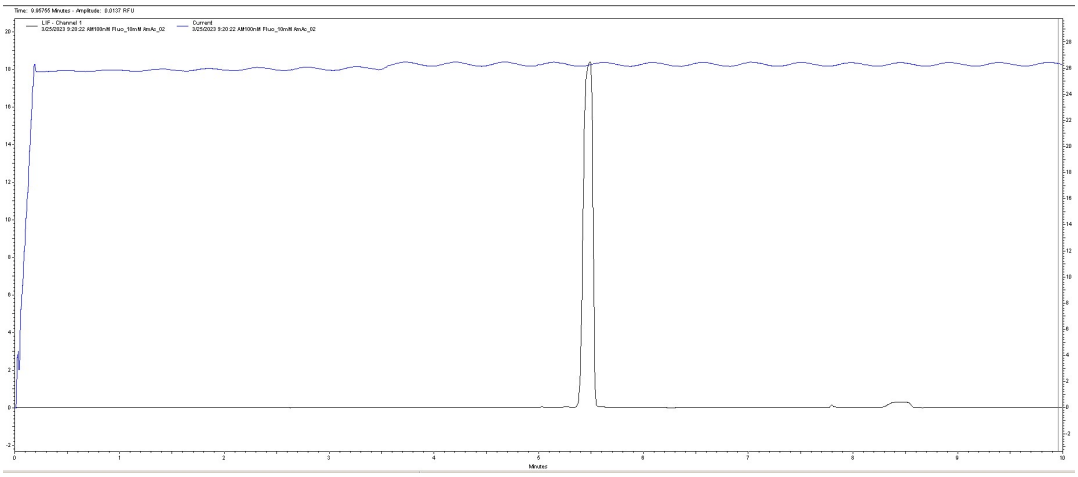

Figure 13. Electropherogram of 100nM fluorescein. Separation of 25KV in 10mM ammonium acetate buffer. Current shown in blue (μA), LIF signal shown in black (RFU).

As the migration time of the tNSP2 aptamer was acceptable, the reproducibility of the migration time was tested. The migration time was seen to be stable, with all replicates migrating at a time of around 7.1 to 7.5 min (Figure 14). The migration time reproducibility is acceptable for K_d determination using CE.

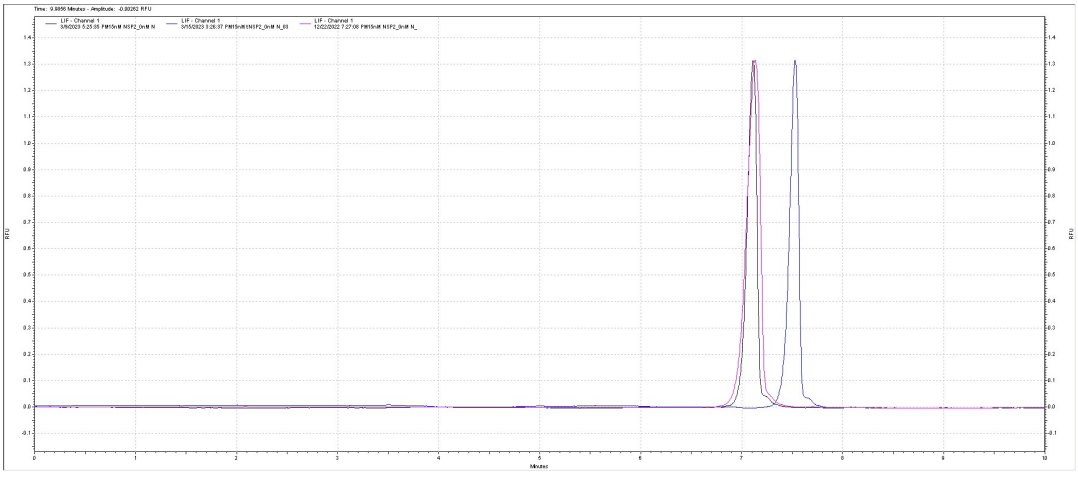

Figure 14. Electropherogram of 15nM tNSP2 aptamer. Separation of 25KV in 10mM ammonium acetate buffer, with replicate one in blue, replicate two in purple and replicate three in black.

Ohm Plot

Performing an Ohm plot is essential for understanding the limits of the developed method and the optimal voltage for separation. The optimal voltage is a function of the capillary diameter,

capillary length, BGE concentration, BGE ionic mobilities, and the temperature of the system and efficiency of the cooling system. A nonlinear increase in current with voltage (Ohm's law) indicates a temperature increase of the buffer in the capillary due to joule heating. Heating is problematic because it can cause non-uniform temperature gradients, local changes in viscosity, and subsequent zone broadening.[22] Therefore, optimal voltage can be determined from the linear range of the Ohm plot (Figure 15). In this case, the plot is linear across all voltages and the selected voltage (25 kV) is suitable. The high voltage allows for better efficiency and resolution while limiting joule heating.

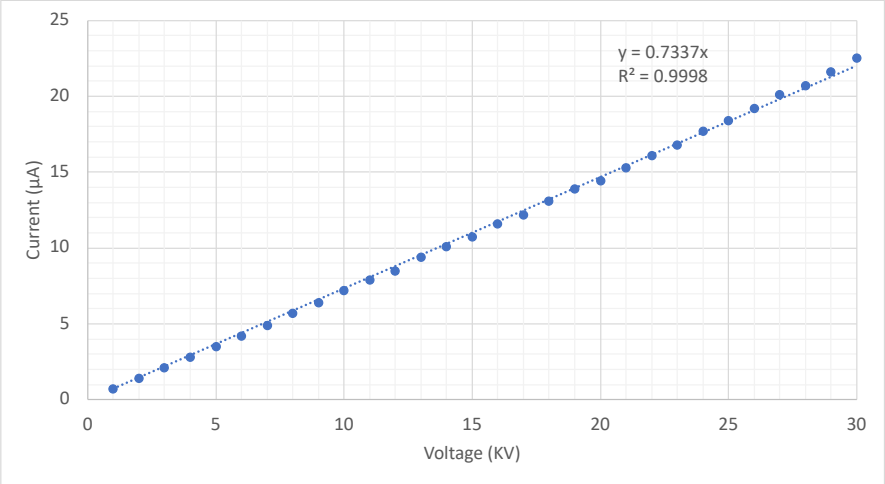

Figure 15. Ohm plot of 10mM ammonium acetate buffer pH 9.00 measured from 1-30KV, 60 cm capillary at 22 ℃.

2.1.4. Conclusions

The optimal buffer was selected to be ammonium acetate pH 9.20 because of the better migration time, MS compatibility, and reproducibility of results. The selected separation voltage (25KV) was determined to be appropriate from the Ohm Plot.

2.2. Sample Vial Coating

2.2.1. Introduction

Biomolecules, such as proteins, have a natural tendency to stick to the surfaces used in sample preparation. The main mechanisms of interactions between biomolecules and surfaces include

electrostatic, hydrophobic, and hydrogen bonding.[30] The amphipathic nature of proteins lends themselves to be readily absorbed via these mechanisms.[31] Unwanted sample-surface interactions can lead to sample degradation and/or sample loss. Preventing protein absorption can be achieved with buffering at extreme pH.[30] However, these pH are not suitable to study proteins in native conditions. Several procedures for reducing sample absorption have been described in the literature. These include the addition of Tween20, adding bovine serum albumin (BSA), coating tubes with polyethylene glycol (PEG), or coating with siliconizing agents.[31–33]

This problem is not unique to proteins: poor reproducibility in CE studies of DNA-protein interactions has been shown to be because of DNA adsorption to reservoir walls.[34] These errors are significantly more pronounced at lower concentrations of DNA and protein.[34] This is explained by the low concentrations of DNA resulting in a larger portion of the DNA molecules which can interact with the available surface area. Vortexing the samples disturbs these interactions and was found to temporarily increase the effective DNA concentration.[34] However, vortexing is impractical for running sequences as you would need to stop the sequence and vortex before each sample. Therefore, a sample-vial-coating approach is preferred.

2.2.2. Methods

Capillary Electrophoresis (CE) Method (NECEEM)

NECEEM was performed with a CE instrument (P/ACE MDQ, Beckman-Coulter) with laser-induced fluorescence (LIF) detection (488 nm excitation, 520 nm emission). An uncoated fused-silica capillary was used with the following dimensions: 60 cm × 75 µm i.d. × 350 µm o.d. The length from the injection end to the detection window was 50 cm. Electrophoresis was run with a positive electrode at the injection end and an electric field of 416 V/cm. The run buffer was 10mM ammonium acetate pH 9.20. The capillary was rinsed with a succession of 1.0 mM SDS, 100 mM HCl, 100mM NaOH, and MS water. The samples were injected with a 0.5 psi pressure for 15 s into the capillary which was prefilled with the run buffer.

Sample Preparation

Samples were prepared consisting of 10nM tNSP2 aptamer and varied concentration of N protein was added. After 30 min incubation at room temperature, the binding was determined by CE. Each sample was run in triplicate. The sample buffer consisted of 5mM ammonium acetate pH 9.00 with the possible addition of Tween80, tRNA, BSA or formic acid. The sample vials were left either uncoated or coated with 2% BSA, followed by a water rinse, and evaporated at 60°C.

2.2.3. Results and Discussion

No coating and no addition to sample buffer

As a baseline referencing guide, the aptamer-protein samples were prepared in the sample buffer with no addition and added to vials with no coating. When the aptamer was incubated with 200 nM N protein, significant complex formation was observed in the electropherogram (Figure 16). Most of the aptamer was bound in the complex, with little to no free aptamer observed. When the protein concentration was dropped to 150nM, no complex peaks were observed (Figure 17). Most of the aptamer migrated as free aptamer. It was expected that decreasing the protein concentration would decrease the complex peaks and increase the free aptamer peaks. Observing either all complex (200nM N sample) or all free aptamer (150nM N sample) was not expected. The rapid switch from complex formation to no complex at a small protein concentration change suggested the occurrence of sample loss. As such, it is not likely that a representative sample plug with 10nM tNSP2 and 150/200nM N protein was being injected into the CE.

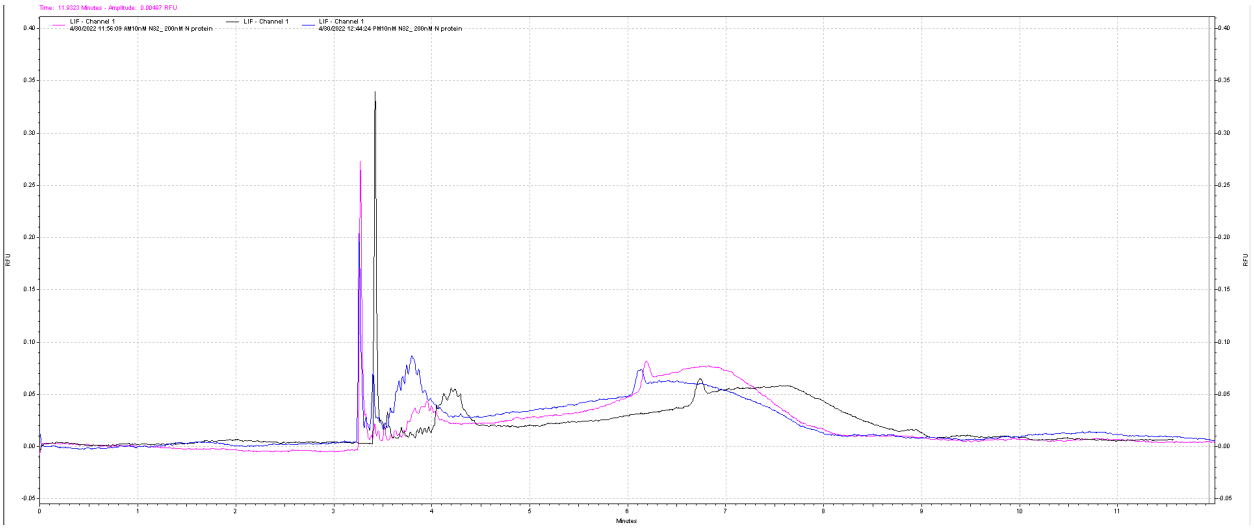

Figure 16. Electropherogram of 10nM tNSP2 aptamer with 200nM N protein prepared in 5mM ammonium acetate and run using no-coating CE sample vials. Complex peaks migrate around 3-4 min while there is little to no free aptamer peaks at around 6-7 min. Replicate one in blue, replicate two in purple and replicate three in black.

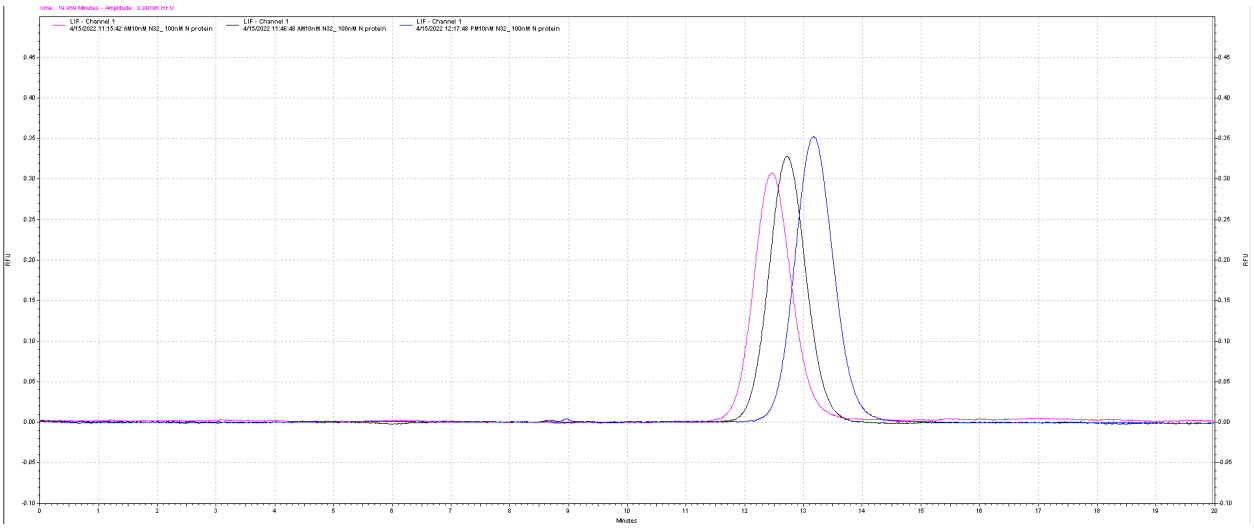

Figure 17 . Electropherogram of 10nM tNSP2 aptamer with 150nM N protein prepared in 5mM ammonium acetate and run using no-coating CE sample vials. Much of the aptamer migrates as free aptamer, with no significant complex peaks. Replicate one in blue, replicate two in purple and replicate three in black.

Sample vial coated with 2% BSA

Sample vials were coated with 2% BSA solution as per the method outlined.[32] The premise of coating the vials with BSA is to limit the amount of vial surface that is available to interact with the aptamer-protein sample. The vials were rinsed with water after coating to remove any BSA

that had not been adsorbed to the walls. When the tNSP2 aptamer was incubated with 150nM N protein, using the coated sample vial, more protein and aptamer were free in solution to interact and bind with each other, as seen in the electropherogram (Figure 18). The faster migrating complex peaks are observed as well as some free aptamer. Compared to the electropherogram of the 200nM N sample (Figure 16), there is a slightly less complex and slightly more free aptamer. This follows the expected trend of decreasing protein concentration.

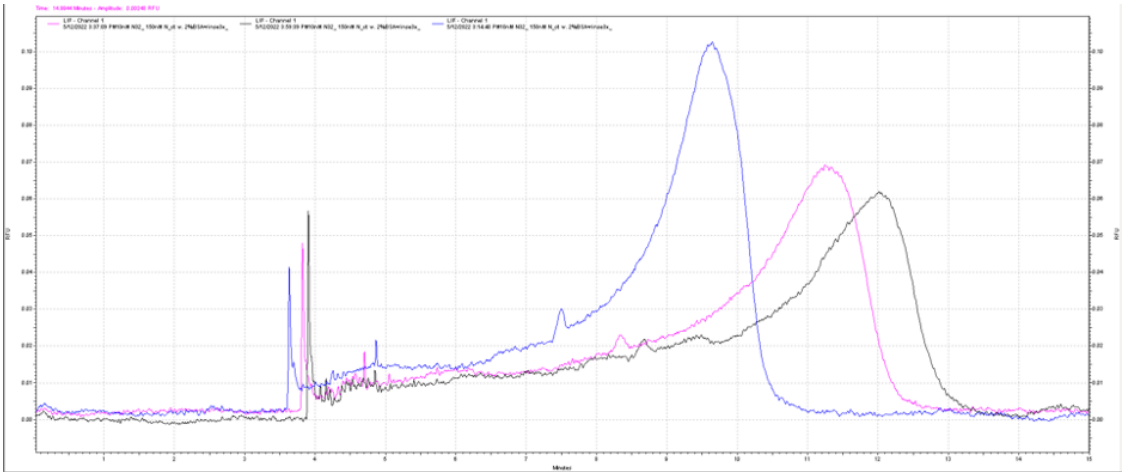

Figure 18. Electropherogram of 10nM tNSP2 aptamer with 150nM N protein prepared in 5mM ammonium acetate and run using 2% BSA coated CE sample vials. The aptamer migrates both as part of the complex, peaks migrating first, followed by the free aptamer peak. Replicate one in blue, replicate two in purple and replicate three in black.

2.2.4. Conclusions

Multiple strategies were tested to limit the sample sticking to the sample vial. This includes 2% BSA coating as well as addition of Tween80, addition of BSA, addition of tRNA, addition of formic acid, and the use of commercial Protein Lobind tubes (Eppendorf™); further details are provided in the appendix. Coating sample vials with 2% BSA followed by three rinses with water and evaporation at 60°C was shown to have minimal sample absorption. This coating procedure was selected for use in CE K_d determination.

2.3. Optimal Ca^{2+} and Mg^{2+} Concentration

2.3.1. Introduction

The binding of aptamers to their target is dependent on the structural conformation of the aptamer. The presence of metal ions affects the aptamer conformation. Alkaline earth metals, such as Mg^{2+} and Ca^{2+}, are known to bind to the phosphate groups on the DNA backbone. They may also bind to the nitrogenous bases, though with less affinity compared to the phosphate groups.[35] The association of metal ions helps stabilize certain conformations of the binding aptamer. This was evidenced using CE to determine the formation of a G-quadruplex upon the addition of K^+, resulting in the correct binding conformation of the thrombin aptamer.[36] Other examples include the stabilization of adenine-sensing riboswitch aptamer via Mg^{2+} and strong Ca^{2+} interaction observed in melting temperature experiments.[37,38]

The selection of aptamer was completed using PBS + 1mM Ca^{2+} + 0.5mM Mg^{2+} pH7.4 buffer. The Ca^{2+} and Mg^{2+} ions were found to play a crucial role in maintaining the affinity of the aptamers to N protein when compared to the buffer with no added ions.[13] As previously mentioned, ionic strength of the buffer impacts EOF and CE separation. Ideally, the selection conditions should be considered when determining K_d. Though the optimal CE run buffer was determined to be ammonium acetate pH 9.20, Ca^{2+} and Mg^{2+} can be added to better simulate selection conditions. The objective of this analysis was to assess the compatibility of SELEX Ca^{2+}/Mg^{2+} conditions on aptamer binding in free-solution CE.

2.3.2. Methods

Sample preparation

A constant concentration of 25nM tNSP2 aptamer and 250nM N protein was prepared in the incubation buffer. The incubation buffer consisted of 5mM ammonium acetate with 0.5 mM Mg^{2+} and varying concentrations of Ca^{2+}. After 30 min incubation at room temperature, binding was determined by CE. Each sample was run in triplicate.

2.3.3. Results and Discussion

To assess the impact of adding divalent cations on aptamer-protein binding in CE, samples were incubated with varied ion concentrations. For simplicity, only Ca^{2+} was varied while Mg^{2+} was kept constant at 0.5 mM (same as the conditions used for SELEX). It is reasonable to assume Ca^{2+} and Mg^{2+} will behave relatively similarly in the CE capillary because both have a +2 charge and differ only in size. Therefore, we can estimate the overall impact of adding divalent cations by adjusting just one species.

Table 1 compares the binding of tNSP2 aptamer to N protein and the resulting complex peaks across the samples with the different Ca^{2+}/Mg^{2+} concentrations. The sample buffer with no added Ca^{2+}/Mg^{2+} showed the smallest complex peak. The most complex was observed in the sample containing 0.5mM $Ca^{2+}$and 0.5 mM Mg^{2+}, with approximately six times greater complex formation compared to the control sample without Ca^{2+}/Mg^{2+}. The sample buffer with SELEX cation concentrations also showed a significant increase (approximately four times) of the complex compared to the control.

Table 1. 25nM tNSP2 aptamer was incubated with 250nM N protein for 30 min prior to checking binding on CE. The maximum peak height of the aptamer-protein complex with varying Ca^{2+} concentrations in sample buffer was noted. Results are listed as mean of triplicate ± standard error.

[Ca^{2+}]	**[Mg^{2+}]**	**Migration Time (min)**	**Peak Height (RFU)**
0 mM	0 mM	2.94 ± 0.07	0.0105 ± 0.0036
0 mM	0.5 mM	2.97 ± 0.17	0.040 ± 0.016
0.25 mM	0.5 mM	3.24 ± 0.13	0.022 ± 0.009
0.5 mM	0.5 mM	2.92 ± 0.10	0.063 ± 0.018
1.0 mM	0.5 mM	2.99 ± 0.08	0.042 + 0.011

2.3.4. Conclusions

Sample buffer containing 0.5mM Mg^{2+} and 1mM Ca^{2+} showed improved binding in CE when compared to the buffer without Mg^{2+} or Ca^{2+}. When comparing samples with 0.5mM Mg^{2+}, the

addition of 0.5mM Ca^{2+} had the largest complex peak height. Nevertheless, 0.5mM Mg^{2+} and 1mM Ca^{2+} were chosen as optimal additions to the sample buffer for K_d determination because of improved binding and closest comparison to SELEX conditions.

3. CE characterization of anti-N aptamers to SARS-CoV-2 N protein

3.1. Introduction

Non-equilibrium CE of equilibrium mixtures (NECEEM) was developed to study ligand-protein binding equilibrium kinetics. Each NECEEM electropherogram provides data for determining K_d and k_{off}.[39] Consequently, k_{on} can be calculated from the K_d and k_{off} relationship. Typically, only one species is labeled; for example, a fluorescently tagged aptamer. This tagging results in a NECEEM electropherogram with a complex peak, free aptamer peak, and dissociated aptamer smear. However, if fluorescence detection is used, the potential fluorescence quenching upon complex formation should be taken into consideration. Due to the species interaction of the fluorescent tagged aptamer with the much larger protein, fluorescence quenching can be experienced within the complex peak.[39,40] To circumvent this, the peak areas can be corrected using a quenching coefficient specific to that complex, or by simply considering only the non-quenched free aptamer peak.

A common way to measure K_d is to titrate a constant concentration of the ligand with an increasing concentration of the target. For example, maintaining a constant concentration of the fluorescent tagged aptamer and varying the protein concentration. Apparent K_d can be estimated from the binding curve using nonlinear regression analysis.[41] This approach would avoid the quenching consideration, but requires multiple electropherograms at different protein concentrations to interpret the K_d value.

The goal of this chapter is to use CE to determine the apparent K_d of the previously selected aptamers to SARS-CoV-2 N protein. The aptamers contained a FAM label at the 5’ end, to allow for CE-LIF (laser-induced-fluorescence) detection. The CE results would then indicate the apparent K_d measured using a homogenous affinity method.

3.2. Methods

3.2.1. Equilibrium Mixture

A constant concentration of 15nM FAM-labelled aptamer and varying concentrations of N protein was prepared in an incubation buffer. The incubation buffer was 5mM ammonium acetate with 0.5 mM Mg^{2+} and 1mM Ca^{2+}. Samples were prepared in 2% BSA coated vials. The aptamer solution was heated to 95°C, the temperature was maintained for 1 min, and this was followed by cooling to 22°C. The desired concentration of N protein was added to the cooled aptamer solution. After 30 min incubation at room temperature, binding was determined by CE.

3.2.2. CE Method (NECEEM)

NECEEM was performed with a CE instrument (P/ACE MDQ, Beckman-Coulter) with laser-induced fluorescence (LIF) detection (488 nm excitation, 520 nm emission). An uncoated fused-silica capillary was used with the following dimensions: 60 cm × 75 µm i.d. × 350 µm o.d. The length from the injection end to the detection window was 50 cm. Electrophoresis was run with a positive electrode at the injection end and an electric field of 416 V/cm. The run buffer was 10mM ammonium acetate at pH 9.3. The capillary was rinsed with a succession of 1.0 mM SDS, 100 mM HCl, 100mM NaOH, and MS water. The samples were injected into the capillary, prefilled with the run buffer, using a 0.5 psi pressure for 15 s. Each sample was run in triplicate.

3.2.3. Determination of Binding Equilibrium Kinetics

The apparent dissociation constant, K_d, was determined by plotting the fraction of bound ligand (aptamer) versus target concentration (N protein). Kd was estimated directly from this binding curve, where the Kd is equivalent to the concentration of N protein at 50% bound aptamer. The fraction bound was calculated as the difference between the total and free ligand concentrations: $[L_{bound}] = [L_{tot}] - [L_{free}]$. The rates of complex formation and dissociation as k_{on} and k_{off}, respectively, were calculated using the NECEEM equations.[39]

3.3. Results and Discussion

3.3.1. CE Detection of Aptamer-Protein Complex

Preliminary tests were performed using 15nM tNPS2 aptamer incubated with N protein to determine the migration of the free aptamer and complex peaks. As can be seen from the stacked electropherogram, there is a clear separation of the migrating complex and free aptamer (Figure 19a). When the electropherograms are viewed on the same scale (Figure 19b), the effect of quenching is evident. Quenching was observed because of the FAM-labelled aptamer binding with the relatively large N protein, with the larger protein partially blocking the signal. Using the areas under each curve, the quenching coefficient was determined. This was repeated for each clone.

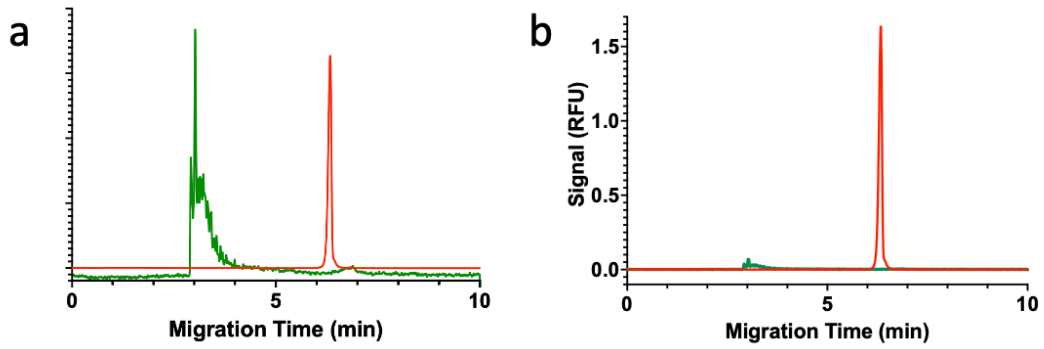

Figure 19. (a) 15nM tNSP2 aptamer incubated with 0 nM N protein in red and with 300nM N protein in green. (b) Stacked electropherograms adjusted to the same y-axis scale, highlighting the effect of quenching for the complex peak (green). When viewed zoomed in the absence of complex in the red electropherogram compared to the appearance of complex peaks in the green electropherogram becomes evident. When the electropherograms are adjusted to the same scale, the presence of quenching is clear in the green complex peaks.

Table 2. Quenching coefficient of FAM-aptamers to SARS-CoV-2 N protein, as measured using CE-LIF. Determined by comparing the free aptamer peak incubated with no protein and the complex peak incubated with a high concentration of protein.

Aptamer	**Quenching Coefficient**
tNSP1	1.6
tNSP2	1.2
tNSP3	1.1

As seen in Table 2, each aptamer clone displayed a similar quenching coefficient. These values were displayed as the average of three replicates. From these preliminary results, the CE method was determined to be adequate for separating the aptamer-protein complex and the free aptamer. However, because of the significant quenching, the complex peak was diminished at the approximated peak height of 0.08 RFU compared to the free aptamer peak of 1.8 RFU (Figure 19b). When considering peak areas, this translated to a quenching coefficient of 1.2. The decreased signal may lead to difficulty in confidently identifying the complex peaks from the baseline value. Hence, it was decided to only consider the free aptamer peak and use varying concentrations of N protein to determine K_d.

3.3.2. Determination of Apparent Kd

To assess the binding of the anti-N clones in capillary electrophoresis, each aptamer was incubated with varying concentrations of N protein from 0nM to 400nM. The resulting electropherograms were analyzed to determine the percent binding for each aptamer-N protein concentration. Binding curves were constructed using GraphPad. The K_d values were determined to be 18 ± 4 nM, 45 ± 11 nM, and 32 ± 7 nM for tNPS1, tNSP2, and tNSP3, respectively (Figure 20, Table 3).

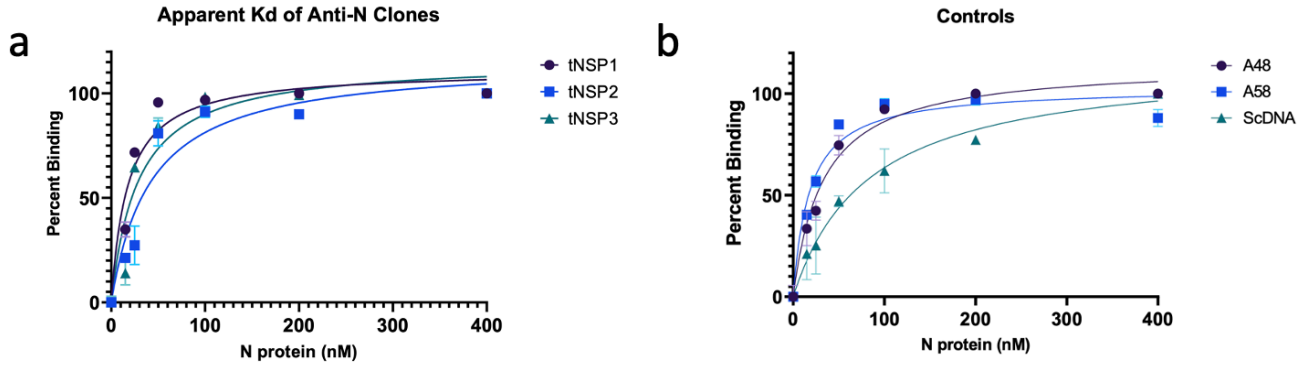

Figure 20. (a) Binding curve of tNSP1, tNSP2, and tNSP3 aptamers with SARS-CoV-2 N protein. (b) Binding curve of positive controls, A48 and A58, and the negative control, ScDNA.

For each aptamer clone, N protein was varied until maximal binding was reached. This was achieved with as little as 200nM N protein (anti-N clones) or up to 400nM N protein (ScDNA). The binding curves are presented in Figure 20. Of the 3 anti-N clones, tNSP1 and tNSP3 showed similar

binding profiles, whereas tNSP2 showed slightly less binding. This is also reflected in the calculated K_d values (

Table 3).

Table 3. Apparent K_d of FAM-aptamers to SARS-CoV-2 N protein, measured using CE-LIF and calculated from the binding curves. Results are shown as the mean of three replicates ± standard error.

Aptamer	**Apparent Kd (nM)**	**R^2**
tNSP1	18 ± 4	0.92
tNSP2	45 ± 11	0.90
tNSP3	32 ± 7	0.90
A48	33 ± 4	0.97
A58	21 ± 2	0.98
ScDNA	88 ± 14	0.96

In addition to the binding assay of the selected anti-N clones, the binding of two positive controls was measured. A48 and A58 are previously published aptamers, with reported K_d values of 0.49 ± 0.95 and 0.70 ± 0.06 nM, respectively.[42] When tested with CE, the clones displayed K_d values of 33 ± 4 and 21 ± 2 nM for A48 and A58, respectively. In both cases, the CE results showed a higher K_d. The difference in the binding kinetics may be related to the experimental aptamer binding conditions. When selecting A48 and A58, a high salt buffer was used to balance the electronegativity of the system.[42] Additionally, a high proportion of serum was added to aid in the specificity and stability of the aptamers. Lastly, the published K_d values were measured using surface plasmon resonance (SPR) in which the N protein was immobilized on the sensor chip.[42] The differences in the buffer as well as the immobilized nature of SPR present a different binding environment compared to CE. The buffer system affects the charge and so the electrostatic interactions of the aptamer-protein complex. Moreover, an aptamer binding to an immobilized protein presents different sterics compared to an aptamer binding to a protein in solution. This

difference might account for the change in K_d measurements between reports in the existing literature and CE experiments.

Scramble DNA (ScDNA) with 64 nucleotides was tested as a negative control. The ScDNA is comprised of a random sequence with no specificity to N protein. ScDNA displayed a K_d of 88 ± 14 nM, about 2-5 times lower affinity than any of the aptamers tested. Although to a lesser extent, ScDNA still binds to N protein despite being a random sequence. This can be assumed to be non-specific binding because of the nature of the target. The N protein is responsible for packaging the viral genome in SARS-CoV-2. The protein contains an RNA binding domain. Furthermore, it is predicted that other N protein domains bind with RNA through nonspecific interactions.[8] Hence it is reasonable to assume that this association and nonspecific interactions can also occur with single-stranded DNA, as evidenced by the ScDNA binding affinity. Nonetheless, all aptamers specific to N protein displayed better affinity than the scramble sequence.

3.3.3. Rate of Association and Dissociation

An ideal CE electropherogram will show visible peaks for free aptamer, aptamer-protein complex, and aptamer dissociated from the complex. Due to the quenching mentioned previously, only the free aptamer peak was used to determine binding affinity. In doing so, multiple concentrations of N protein were incubated with the aptamers resulting in different complex, dissociation, and free aptamer peak profiles. If a single concentration of N protein gave an electropherogram in which all 3 types of peaks can be identified, then NECEEM equations can be applied. From the electropherogram, k_{off} was determined. Then the relationship between K_d and k_{off} was used to calculate k_{on} (Table 4).

Table 4. Rates of association (k_{on}) and dissociation (k_{off}) of the anti-N clones. Calculated from the NECEEM electropherograms. Values are shown as the mean of three replicates ± standard error.

Aptamer	**k_{on}** (1/M·s)	**k_{off}** (1/s)
tNSP1	3.22 ± 1.02 x 10^{-6}	3.73 ± 1.20 x 10^{-3}

tNSP2	$6.85 \pm 3.59 \times 10^{-6}$	$5.81 \pm 2.45 \times 10^{-3}$
tNSP3	$2.45 \pm 1.14 \times 10^{-6}$	$1.05 \pm 0.48 \times 10^{-3}$

3.4. Conclusions

Altogether, 5 aptamers specific to N protein as well as ScDNA were assessed for binding to N protein. The selected aptamers (tNSP1, tNSP2, and tNSP3) exhibited a high binding affinity to N protein with tNSP1 having the highest affinity of 18 ± 4 nM. Both A48 and A58, clones from the existing literature, displayed K_d values within the same range as the three selected aptamers. While the ScDNA displayed some binding, it had many times lower affinity compared to the 5 N protein specific aptamers.

4. BLI characterization of anti-N aptamers to SARS-CoV-2 N protein

4.1. Introduction

The aim of the overall thesis is to characterize the binding of aptamers to SARS-CoV-2 nucleocapsid (N) protein using CE and compare it with the BLI characterization. The apparent Kd of the anti-N aptamers was determined using CE above. In doing so, the assay conditions were optimized for the CE system. To compare BLI and CE, an effort should be made to keep as many variables as possible the same across the two techniques. In this sense, the CE assay conditions should be used to test the aptamer clones on a BLI system. Additionally, the initial SELEX to obtain the aptamers was completed using BLI. The SELEX conditions were suitable for the BLItz system and can also be used to determine K_d.[13]

The goal of this chapter is to use BLI to determine the apparent K_d of the previously selected aptamers to SARS-CoV-2 N protein. The aptamers contained a biotin label at the 5’ end, to allow for immobilization on the streptavidin biosensors. The BLI results would indicate the apparent K_d measured using a heterogenous affinity method.

4.2. Methods

4.2.1. Determination of Binding using BLItz Label-Free Biosensor System

BLItz label-free biosensor system for biolayer interferometry assay (ForteBio, USA) was used to test for binding of the aptamers to SARS-CoV-2 N protein. Briefly, biotinylated aptamers were loaded onto a streptavidin biosensor (120 s) for immobilization. After 60s waiting for the baseline to stabilize, the association was performed by loading SARS-CoV-2 N protein solution onto the sensor. The association and dissociation events were recorded for 150s each. The solutions and timings of each of the events are listed in Table 5. All solutions were prepared in an assay buffer, which was either 5 mM ammonium acetate 1mM Ca^{2+} 0.5 mM Mg^{2+} pH 9.0, or PBS 0.05% Tween20 1mM Ca^{2+} 0.5 mM Mg^{2+}.

Table 5. BLItz method for screening for binding.

Step	Time	Drop/Tube	Sample
Initial baseline	60s	Tube	Assay buffer
Loading	120s	Tube	400nM aptamer
Baseline	60s	Tube	Assay buffer
Association	150s	Tube	38.91 to 155.6 nM N protein
Dissociation	150s	Tube	Assay buffer

4.2.2. Determination of Non-specific Binding (NSB) using BLItz Label-Free Biosensor System

The BLItz label-free biosensor system for biolayer interferometry assay (ForteBio, USA) was used to determine the non-specific binding (NSB) of the aptamer clones. The method followed a similar protocol as the screening method apart from the loading step. To test for NSB, the PBS buffer solution was incubated with the biosensor during the loading step. The steps are listed in Table 6.

Table 6. BLItz NSB method, noting the change of the loading step to using assay buffer.

Step	Time	Drop/Tube	Sample
Initial baseline	60s	Tube	Assay buffer
Loading	120s	Tube	Assay buffer
Baseline	60s	Tube	Assay buffer
Association	150s	Tube	155.6 nM N protein
Dissociation	150s	Tube	Assay buffer

4.3. Results and Discussion

4.3.1. Determination of Apparent Kd in Ammonium Acetate

The tNSP3 aptamer was selected as a test sample to compare CE running conditions using the BLItz system. The assay buffer was 5 mM ammonium acetate 1mM Ca^{2+} 0.5 mM Mg^{2+} pH 9.20, using the same solution as the sample buffer for CE. Three different protein concentrations were tested and, from the sensorgram, a change in interference was observed during association (Figure 21). The change in interference corresponds to a change in the thickness of the biolayer, which suggests the association of N protein to the immobilized aptamer. There was a decrease in binding observed with a decrease in protein concentration.

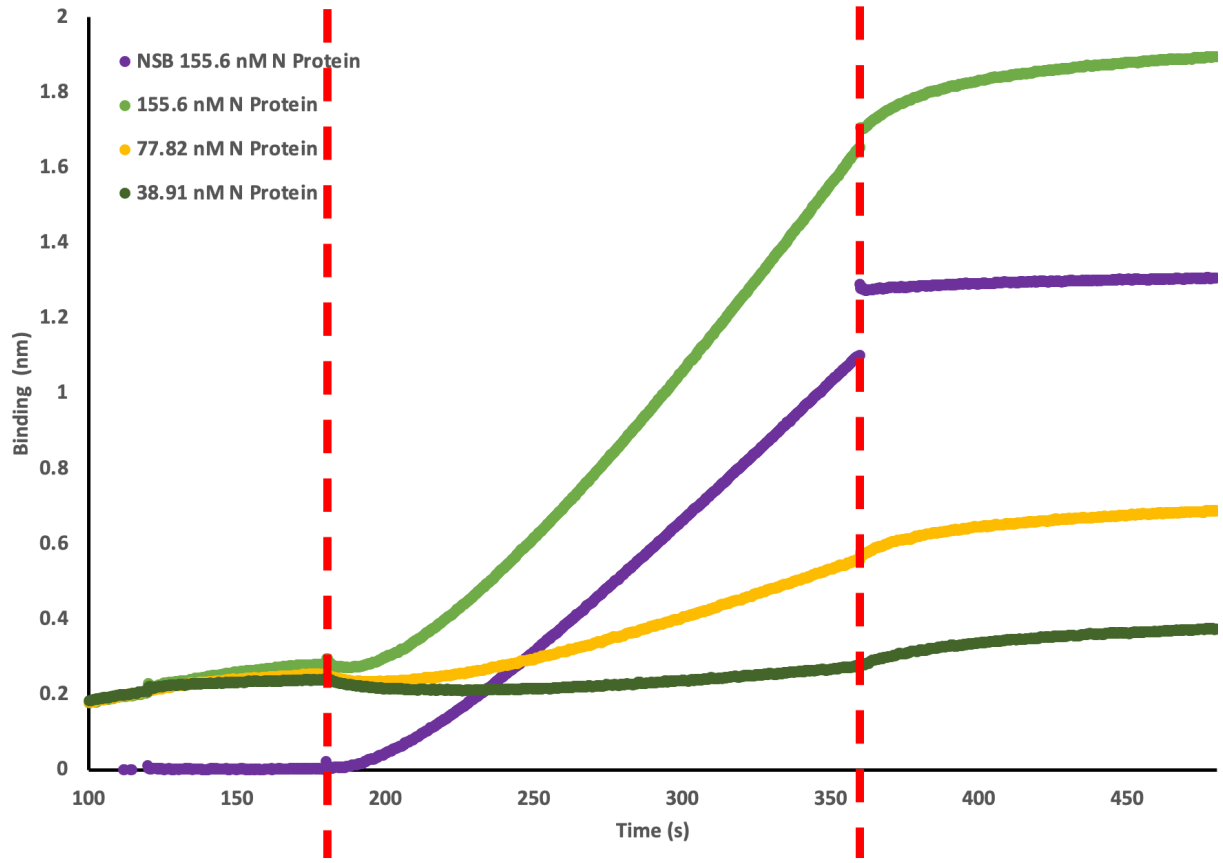

Figure 21. Sensorgram of tNSP3 aptamer immobilized to streptavidin biosensor and association with N protein. NSB sensorgram is shown in purple. The sensorgram is divided by a dotted red line to indicate the baseline, association, and dissociation steps (left to right).

The NSB test was conducted in which no aptamer was immobilized on the biosensor. For NSB, any observed association would correspond to the N protein interacting directly with the streptavidin biosensor. Unexpectedly, significant NSB was observed (Figure 21). To account for NSB, the association of NSB can be used as a reference to 'zero' the sensorgrams prior to Kd calculation.[13] However, this is not ideal because there is a greater association in the NSB run compared to most of the sample runs. Only the highest concentration of N protein (155.6nM N protein) showed a greater association of protein to the immobilized aptamer compared to the NSB association of protein to the biosensor.

To suppress NSB, 0.2% BSA and 0.05% Tween20 were added to the assay buffer. The NSB test was redone using the new buffer (Figure 22). In the new buffer NSB test, an even greater association was than in the highest concentration of N protein tested. Significant NSB suggests

that adjusting the concentration of BSA or Tween20 would most likely not be sufficient, rather the issue may stem from the assay buffer.[13,43] When considering the pH of the assay buffer, it is possible that the biosensor and protein are associating due to high electrostatic interactions. As a result of the significant NSB, CE conditions were found to be unsuitable for the BLItz system. A K_d value could not be determined from these results.

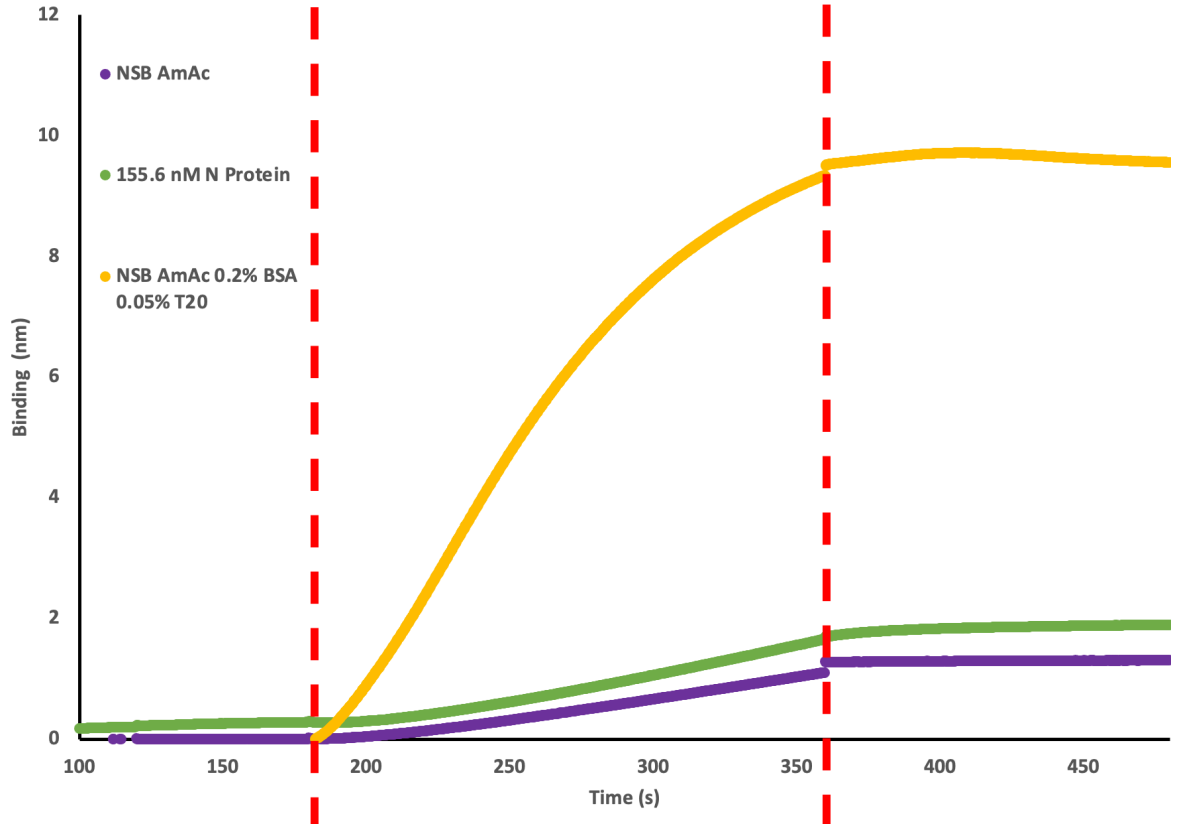

Figure 22. Sensorgrams comparing the presence of NSB in different assay buffers, in comparison to the association of 155.6 nM N protein to immobilized tNSP3 aptamer (green curve). AmAc is used to denote ammonium acetate. The sensorgram is divided by a dotted red line to indicate the baseline, association, and dissociation steps (left to right).

4.3.2. Determination of Apparent Kd in PBS

When the clones were selected, the kinetics of binding were also measured. This was completed in SELEX conditions where the assay buffer was PBS. The K_d, K_{on}, and K_{off} values are reported in Table 7.[13] In this case, biotinylated aptamers were immobilized on streptavidin biosensors, then the biosensors were dipped in N protein solution, and finally binding was measured.

Table 7. Apparent K_d of FAM-aptamers to SARS-CoV-2 N protein, as measured using BLItz and calculated using a 1:1 binding model. Values are shown as the mean of three replicates ± standard error.

Aptamer	**Apparent K_d (nM)**	**k_{on}** (1/M·s)	**k_{off}** (1/s)
tNSP1	4.83 ± 0.63	$1.67 \pm 0.04 \times 10^{5}$	$8.05 \pm 0.15 \times 10^{-4}$
tNSP2	4.51 ± 0.87	$1.25 \pm 0.10 \times 10^{6}$	$5.63 \pm 0.30 \times 10^{-4}$
tNSP3	2.91 ± 0.59	$1.05 \pm 0.01 \times 10^{5}$	$3.05 \pm 0.04 \times 10^{-4}$
A48	6.46 ± 0.60	-	-
A58	3.02 ± 0.55	-	-

4.4. Conclusions

The BLItz label-free biosensor system for biolayer interferometry assay (ForteBio, USA) was used to test binding aptamers to SARS-CoV-2 N protein. After testing for non-specific binding, the CE buffer was found to be ill-suited for use with the BLItz system. This suggests PBS is ideal for the BLItz system while ammonium acetate is ideal for the CE system. The K_d values in PBS were found to be 4.83 ± 0.63, 4.51 ± 0.87, and 2.91 ± 0.59 nM for tNSP1, tNSP2, and tNSP3 respectively.

5. Conclusions and Directions for Future Work

4.1. Conclusions

The CE method developed in Chapter 2 was able to fully separate the free aptamer from the aptamer-protein complex. Sample loss was limited by coating the sample vial with BSA. With the developed method, the binding of FAM-labeled aptamers to N protein was measured. K_d values were determined to be 18 ± 4 nM, 45 ± 11 nM, and 32 ± 7 nM for tNPS1, tNSP2, and tNSP3 respectively. Additionally, the literature clones A48 and A58 (with reported K_d values of 0.49 ± 0.95 and 0.70 ± 0.06 nM) displayed K_d of 33 ± 4 and 21 ± 2 nM, respectively.

Subsequently, the BLItz label-free biosensor system was used to test binding aptamers to N protein. After testing for non-specific binding, the CE buffer was found to be inappropriate for

the BLItz system. The non-compatibility of the CE buffer with the BLI system was deemed to be a result of the higher pH buffer. This suggests, PBS is ideal for the BLItz system while ammonium acetate is ideal for the CE system. The K_d values in PBS using BLI were found to be 4.83 ± 0.63, 4.51 ± 0.87, and 2.91 ± 0.59 nM, for tNSP1, tNSP2 and tNSP3, respectively.

The CE results showed a higher K_d across all aptamers tested. The difference may be related to the experimental aptamer binding conditions. Between CE and BLI, the assay buffer was different as well the binding was either all in solution or with one species immobilized. The buffer system affects the charge and therefore the electrostatic interactions of the aptamer-protein complex. The pH of the buffer would influence the charge of the aptamer and protein. Additionally, the buffer composition may play a role in stabilizing a specific aptamer structure. All aptamers in PBS displayed greater binding, which suggests that PBS may promote a more stable aptamer structure that will bind better to the target protein. Moreover, an immobilized aptamer binding to a protein presents different sterics compared to an aptamer binding to a protein in solution.

By working with these two methods, the advantages and disadvantages of the respective methods were identified. BLI provides a straightforward workflow and simple separation of a complex from the individual species. However, the immobilizing of the biomolecule introduces a surface where nonspecific binding may occur leading to inaccuracies in K_d determination. Additionally, the immobilization itself may impact binding affinity. On the other hand, CE offers a homogenous affinity assay, though the assay conditions must be optimized to allow for the separation of the complex from the individual species. The two methods contrast with each other: BLI has a rigid, immobilized constituent while CE has both binding molecules free in solution. Due to these differences, to evaluate the binding of an aptamer to a target protein it is better to use both methods. This work offers insight into aptamer affinity when the aptamer used in a different system from which it was selected. This work would lead to a better understanding when utilising aptamers from the literature.

4.2. Limitations and Directions for Future Work

There are certain limitations present with this research thesis. As mentioned previously, the buffer conditions vary between the two selected methods. Because the pH of the system differs, the charges of the aptamer-protein may differ, which will impact the stability of their structures. Consequently, the affinity of the aptamer to protein will be impacted. This results in an additional variable that should be considered when making inferences comparing the two methods. As such the comparisons of the two methods should include the entire CE or BLI systems, encompassing instrumentation, sample preparation, and buffer composition. Secondly, all K_d calculations assumed a 1:1 binding of aptamer to protein; this assumption can be verified in future studies. One simple test would be to use CE-MS. The CE method developed in this thesis uses a MS-compatible buffer, therefore this method can be transferred to MS detection with relative ease. The MS spectrum would allow the determination of the aptamer-to-protein binding ratio and whether the 1:1 binding assumption was valid.

Additionally, future studies using different aptamers could provide another comparison of CE and BLI. In this thesis, aptamers were selected using an immobilization technique and were evidenced to have greater binding when using BLI compared to CE. In the future, aptamers can be selected using CE-SELEX and then compared using the two methods. This would further speak to the impact of SELEX conditions on the binding equilibrium kinetics when measured using different methods.

References

1. El-Sadr, W. M., Vasan, A. & El-Mohandes, A. Facing the New Covid-19 Reality. *N. Engl. J. Med.* **388**, 385–387 (2023).
2. Feng, W. *et al.* Molecular Diagnosis of COVID-19: Challenges and Research Needs. *Anal. Chem.* **92**, 10196–10209 (2020).
3. Li, H., Liu, S.-M., Yu, X.-H., Tang, S.-L. & Tang, C.-K. Coronavirus disease 2019 (COVID-19): current status and future perspectives. *Int. J. Antimicrob. Agents* **55**, 105951 (2020).
4. Dzuvor, C. K. O., Tettey, E. L. & Danquah, M. K. Aptamers as promising nanotheranostic tools in the COVID -19 pandemic era. *WIREs Nanomedicine Nanobiotechnology* **14**, (2022).
5. Krammer, F. SARS-CoV-2 vaccines in development. *Nature* **586**, 516–527 (2020).
6. Shan, D. *et al.* N-protein presents early in blood, dried blood and saliva during asymptomatic and symptomatic SARS-CoV-2 infection. *Nat. Commun.* **12**, 1931 (2021).
7. Xu, J. *et al.* Nanobodies from camelid mice and llamas neutralize SARS-CoV-2 variants. *Nature* **595**, 278–282 (2021).
8. Cubuk, J. *et al.* The SARS-CoV-2 nucleocapsid protein is dynamic, disordered, and phase separates with RNA. *Nat. Commun.* **12**, 1936 (2021).
9. Chang, C.-K. *et al.* Multiple Nucleic Acid Binding Sites and Intrinsic Disorder of Severe Acute Respiratory Syndrome Coronavirus Nucleocapsid Protein: Implications for Ribonucleocapsid Protein Packaging. *J. Virol.* **83**, 2255–2264 (2009).
10. Grossoehme, N. E. *et al.* Coronavirus N Protein N-Terminal Domain (NTD) Specifically Binds the Transcriptional Regulatory Sequence (TRS) and Melts TRS-cTRS RNA Duplexes. *J. Mol. Biol.* **394**, 544–557 (2009).

11. Cui, L. *et al.* The Nucleocapsid Protein of Coronaviruses Acts as a Viral Suppressor of RNA Silencing in Mammalian Cells. *J. Virol.* **89**, 9029–9043 (2015).
12. Jayaram, H. *et al.* X-Ray Structures of the N- and C-Terminal Domains of a Coronavirus Nucleocapsid Protein: Implications for Nucleocapsid Formation. *J. Virol.* **80**, 6612–6620 (2006).
13. Poolsup, S. *et al.* Discovery of DNA aptamers targeting SARS-CoV-2 nucleocapsid protein and protein-binding epitopes for label-free COVID-19 diagnostics. *Mol. Ther. - Nucleic Acids* **31**, 731–743 (2023).
14. Kevadiya, B. D. *et al.* Diagnostics for SARS-CoV-2 infections. *Nat. Mater.* **20**, 593–605 (2021).
15. Mathuria, J. P., Yadav, R., & Rajkumar. Laboratory diagnosis of SARS-CoV-2 - A review of current methods. *J. Infect. Public Health* **13**, 901–905 (2020).
16. Wandtke, T. *et al.* Aptamers—Diagnostic and Therapeutic Solution in SARS-CoV-2. *Int. J. Mol. Sci.* **23**, 1412 (2022).
17. Berezovski, M. V., Musheev, M. U., Drabovich, A. P., Jitkova, J. V. & Krylov, S. N. Non-SELEX: selection of aptamers without intermediate amplification of candidate oligonucleotides. *Nat. Protoc.* **1**, 1359–1369 (2006).
18. Mironov, V. *et al.* Structure- and Interaction-Based Design of Anti-SARS-CoV-2 Aptamers. *Chem. – Eur. J.* **28**, (2022).
19. Zhuo, Z. *et al.* Recent Advances in SELEX Technology and Aptamer Applications in Biomedicine. *Int. J. Mol. Sci.* **18**, 2142 (2017).
20. Galievsky, V. A., Stasheuski, A. S. & Krylov, S. N. Capillary Electrophoresis for Quantitative Studies of Biomolecular Interactions. *Anal. Chem.* **87**, 157–171 (2015).

21. Krylov, S. N. Kinetic CE: Foundation for homogeneous kinetic affinity methods. *ELECTROPHORESIS* **28**, 69–88 (2007).
22. Henk H. Lauer & Gerard P. Rozing. *High Performance Capillary Electrophoresis: A Primer*. (Agilent Technologies, 2018).
23. Butler, J. M. Capillary Electrophoresis. in *Advanced Topics in Forensic DNA Typing* 141–165 (Elsevier, 2012). doi:10.1016/B978-0-12-374513-2.00006-3.
24. Kamat, V. & Rafique, A. Designing binding kinetic assay on the bio-layer interferometry (BLI) biosensor to characterize antibody-antigen interactions. *Anal. Biochem.* **536**, 16–31 (2017).
25. Petersen, R. Strategies Using Bio-Layer Interferometry Biosensor Technology for Vaccine Research and Development. *Biosensors* **7**, 49 (2017).
26. Shah, N. B. & Duncan, T. M. Bio-layer Interferometry for Measuring Kinetics of Protein-protein Interactions and Allosteric Ligand Effects. *J. Vis. Exp.* 51383 (2014) doi:10.3791/51383.
27. Petrov, A., Okhonin, V., Berezovski, M. & Krylov, S. N. Kinetic Capillary Electrophoresis (KCE): A Conceptual Platform for Kinetic Homogeneous Affinity Methods. *J. Am. Chem. Soc.* **127**, 17104–17110 (2005).
28. Konermann, L. Addressing a Common Misconception: Ammonium Acetate as Neutral pH "Buffer" for Native Electrospray Mass Spectrometry. *J. Am. Soc. Mass Spectrom.* **28**, 1827–1835 (2017).
29. Gomes, F. P. & Yates, J. R. Recent trends of capillary electrophoresis-mass spectrometry in proteomics research. *Mass Spectrom. Rev.* **38**, 445–460 (2019).

30. Williams, S. & Venkateswaran, N. Assessing Stability, Durability, and Protein Adsorption Behavior of Hydrophilic Silane Coatings in Glass Microchannels. *J. Anal. Bioanal. Tech.* **7**, (2016).
31. Goebel-Stengel, M., Stengel, A., Taché, Y. & Reeve, J. R. The importance of using the optimal plasticware and glassware in studies involving peptides. *Anal. Biochem.* **414**, 38–46 (2011).
32. Felgner, P. L. & Wilson, J. E. Hexokinase binding to polypropylene test tubes. *Anal. Biochem.* **74**, 631–635 (1976).
33. Maes, K., Smolders, I., Michotte, Y. & Van Eeckhaut, A. Strategies to reduce aspecific adsorption of peptides and proteins in liquid chromatography–mass spectrometry based bioanalyses: An overview. *J. Chromatogr. A* **1358**, 1–13 (2014).
34. Kanoatov, M. & Krylov, S. N. DNA Adsorption to the Reservoir Walls Causing Irreproducibility in Studies of Protein–DNA Interactions by Methods of Kinetic Capillary Electrophoresis. *Anal. Chem.* **83**, 8041–8045 (2011).
35. Girardot, M., Gareil, P. & Varenne, A. Interaction study of a lysozyme-binding aptamer with mono- and divalent cations by ACE. *ELECTROPHORESIS* **31**, 546–555 (2010).
36. Szilagyi, A., Bonn, G. K. & Guttman, A. Capillary gel electrophoresis analysis of G-quartet forming oligonucleotides used in DNA–protein interaction studies. *J. Chromatogr. A* **1161**, 15–21 (2007).
37. Reuss, A. J., Vogel, M., Weigand, J. E., Suess, B. & Wachtveitl, J. Tetracycline Determines the Conformation of Its Aptamer at Physiological Magnesium Concentrations. *Biophys. J.* **107**, 2962–2971 (2014).

38. Shlaferman, J., Paige, A., Meserve, K., Miech, J. A. & Gerdon, A. E. Selected DNA Aptamers Influence Kinetics and Morphology in Calcium Phosphate Mineralization. *ACS Biomater. Sci. Eng.* **5**, 3228–3236 (2019).

39. Krylov, S. N. Kinetic CE: Foundation for homogeneous kinetic affinity methods. *ELECTROPHORESIS* **28**, 69–88 (2007).

40. Quenching of Fluorescence. in *Principles of Fluorescence Spectroscopy* (ed. Lakowicz, J. R.) 277–330 (Springer US, 2006). doi:10.1007/978-0-387-46312-4_8.

41. Jing, M. & Bowser, M. T. Methods for measuring aptamer-protein equilibria: A review. *Anal. Chim. Acta* **686**, 9–18 (2011).

42. Zhang, L. *et al.* Discovery of sandwich type COVID-19 nucleocapsid protein DNA aptamers. *Chem. Commun.* **56**, 10235–10238 (2020).

43. Dubrow, A., Zuniga, B., Topo, E. & Cho, J.-H. Suppressing Nonspecific Binding in Biolayer Interferometry Experiments for Weak Ligand–Analyte Interactions. *ACS Omega* **7**, 9206–9211 (2022).

Appendix

Other sample vial coating methods:

The addition of Tween80 showed complex peaks as well as possible free aptamer peaks. However, due to migration shift it is unclear whether the latest migrating peak corresponds with free aptamer or either a contaminant or a nonbinding self-dimer peak.

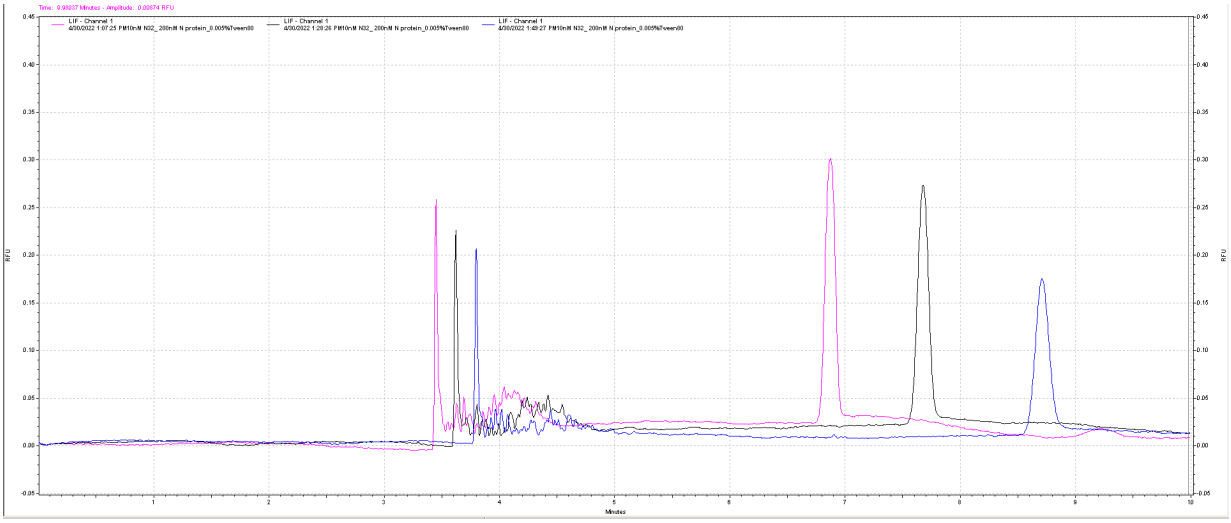

Figure S1. 10nM tNSP2 incubated with 200nM N protein. Sample buffer contained 0.005%Tween80. Replicate one in blue, replicate two in purple and replicate three in black.

The addition of 1mg/mL of BSA in the sample buffer resulted in no complex formation and widening of the free aptamer peak.

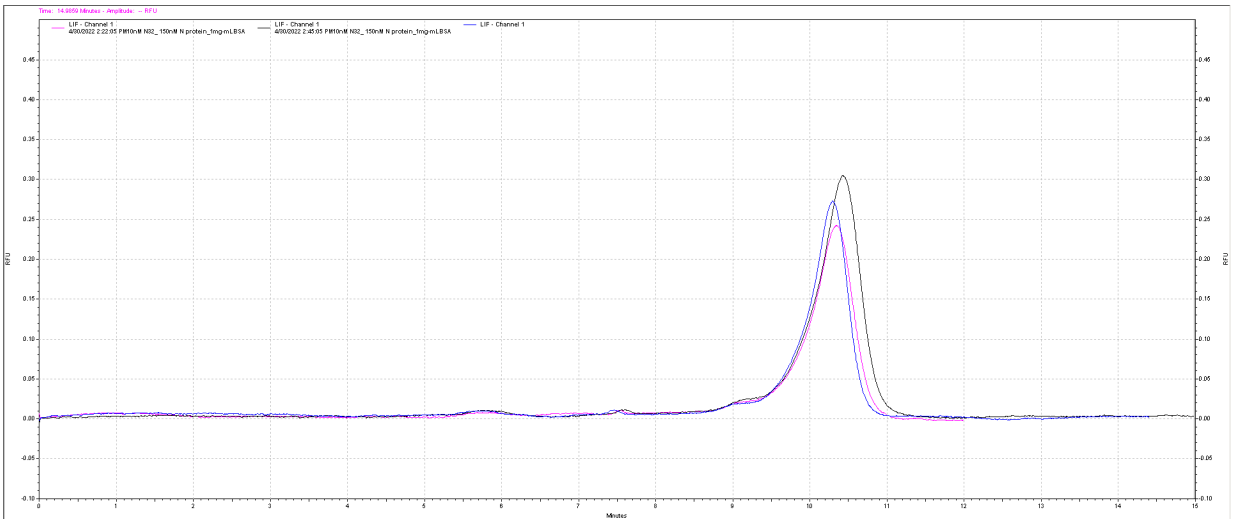

Figure S2. 10nM tNSP2 incubated with 150nM N protein. Sample buffer contained 1mg/mL BSA. Replicate one in blue, replicate two in purple and replicate three in black.

Coating the sample vial with tRNA, followed by water rinse in triplicate resulted in an electropherogram with minimal complex peaks and significant fronting free aptamer peak. In comparison, the same procedure was repeated by increasing the protein to 200nM N protein (Figure S4). With the higher concentration, there is significant complex formation. This suggests the drop in complex formation with 150nM N protein is not due to the addition of tRNA but more likely due to sample loss to the sample vial.

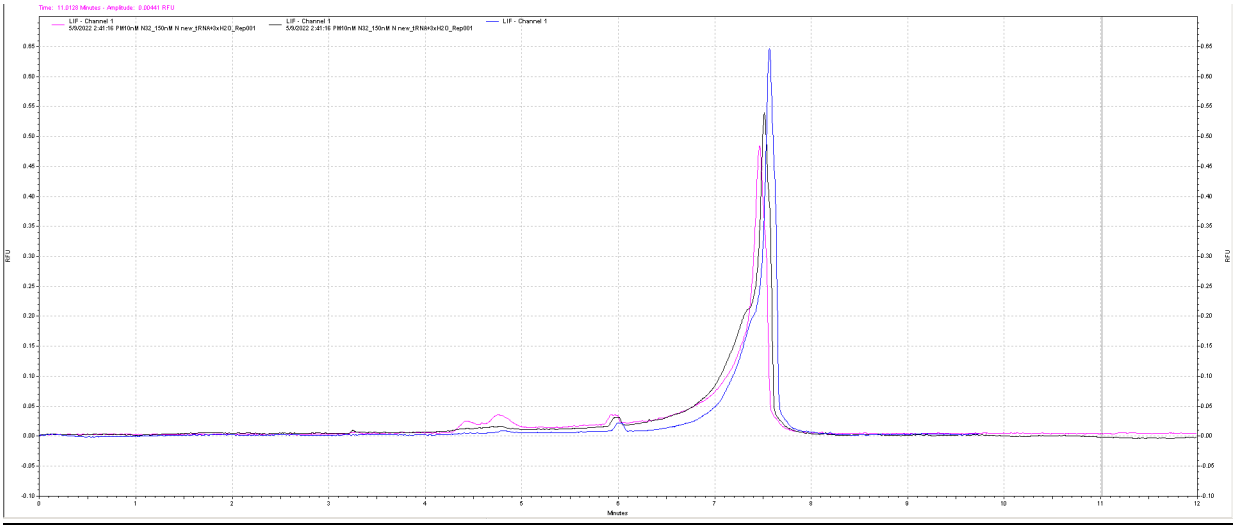

Figure S3. 10nM tNSP2 incubated with 150nM N protein. Sample vial was coated with tRNA. Replicate one in blue, replicate two in purple and replicate three in black.

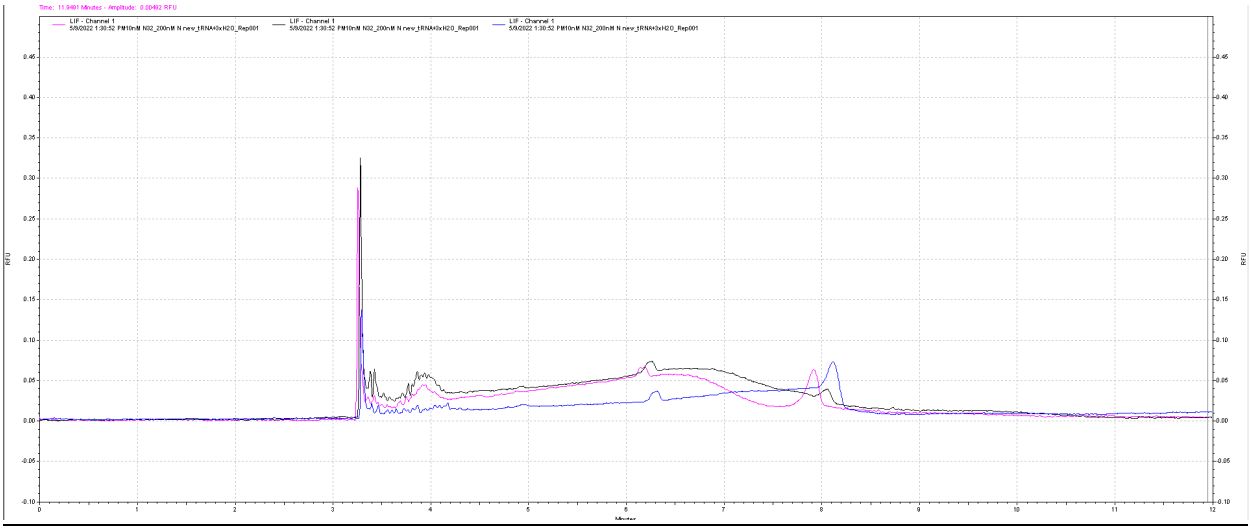

Figure S4. 10nM tNSP2 incubated with 200nM N protein. The sample vial was coated with tRNA. Replicate one in blue, replicate two in purple and replicate three in black.

The addition of 1%BSA to the sample buffer resulted in an electropherogram with no complex peaks. The appearance of a faster migrating shoulder peak was seen with the free aptamer peak.

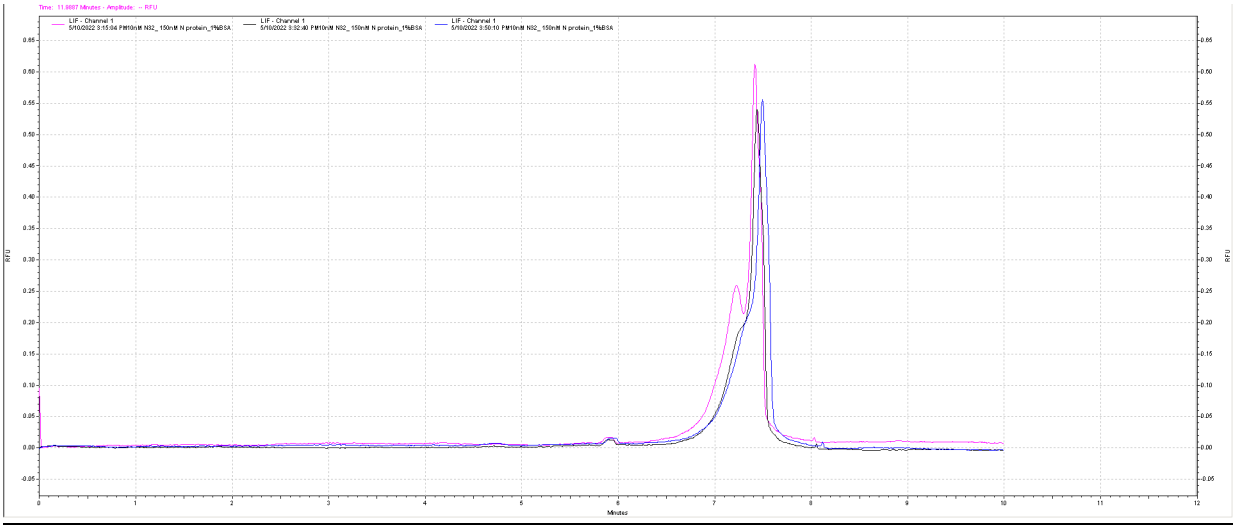

Figure S5. 10nM tNSP2 incubated with 150nM N protein. The sample buffer contained 1% BSA. Replicate one in blue, replicate two in purple and replicate three in black.

Any addition of formic acid (FA) results in no complex formation. Even with increasing the protein concentration to 200nM no complex was observed. This suggests FA prevents complex binding.

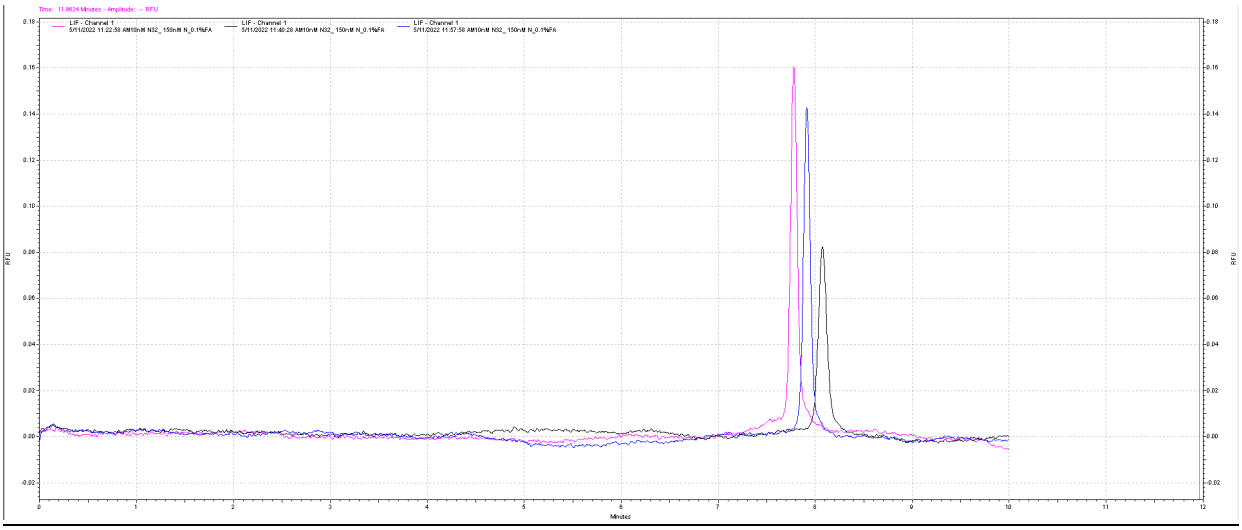

Figure S6. 10nM tNSP2 incubated with 150nM N protein. The sample buffer contained 0.1%FA. Replicate one in blue, replicate two in purple and replicate three in black.

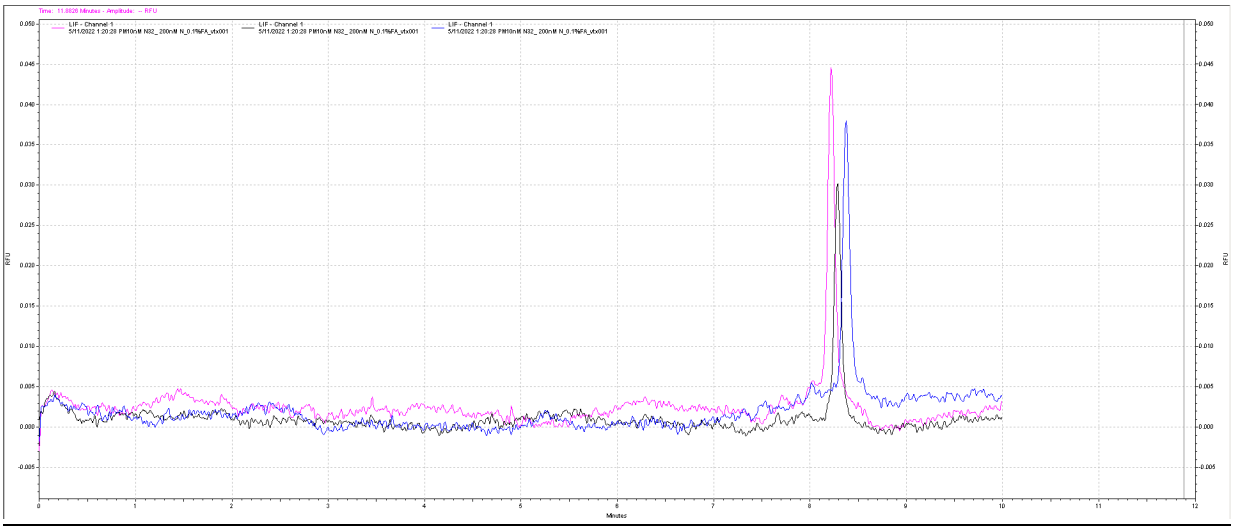

Figure S7. 10nM tNSP2 incubated with 200nM N protein. The sample buffer contained 0.1%FA. Replicate one in blue, replicate two in purple and replicate three in black.

Lastly, commercial tubes designed to be low binding were tested. Samples were prepared in Protein LoBind tubes (Eppendorf™). The sample buffer contained no additions. As seen in Figure S8 the sample with 200nM N protein showed significant complex formation. However, when the protein concentration is decreased to 150nM, the complex disappears (Figure S9). As such, the commercial tubes were not sufficient in preventing sample loss to the tubes.

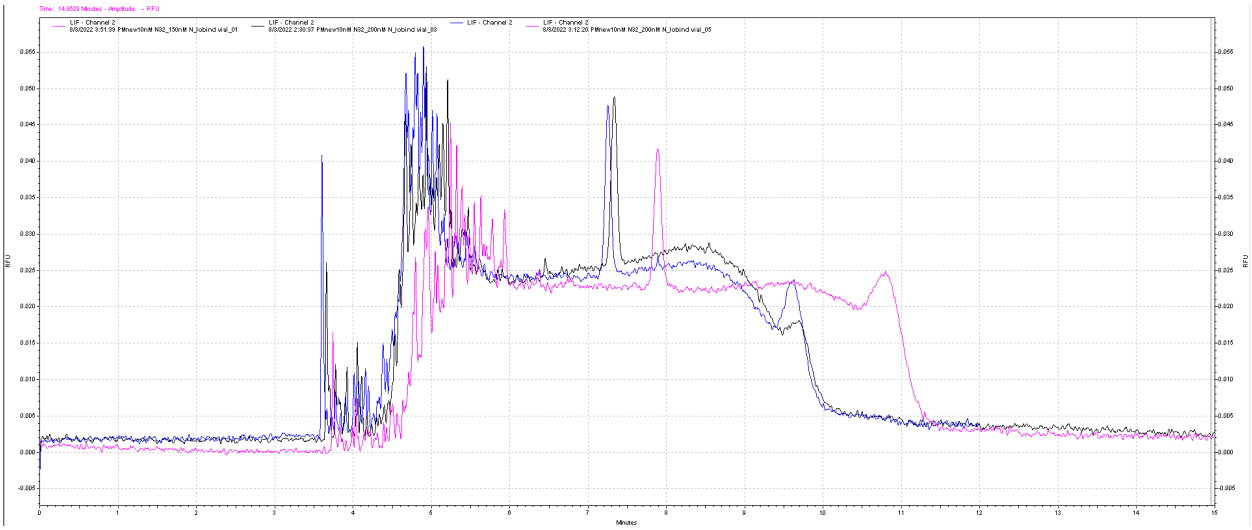

Figure S8. 10nM tNSP2 incubated with 200nM N protein prepared using commercial LoBind tubes. Replicate one in blue, replicate two in purple and replicate three in black.

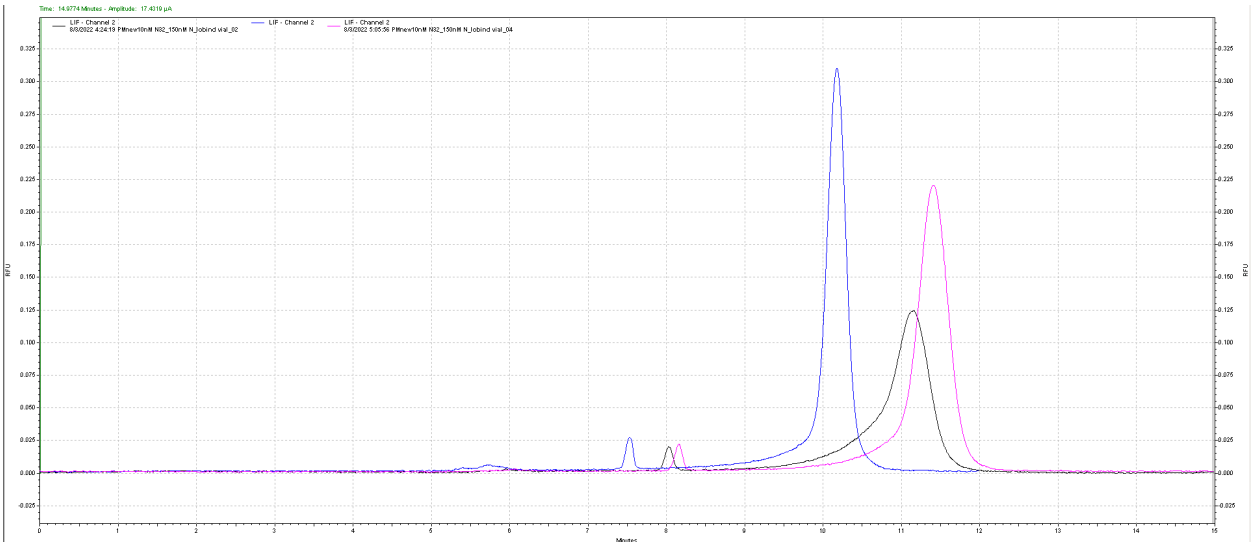

Figure S9. 10nM tNSP2 incubated with 150nM N protein prepared using commercial LoBind tubes Replicate one in blue, replicate two in purple and replicate three in black.